



Understanding the effect of Prandtl number on momentum and scalar mixing rates in neutral and stably stratified flows using gradient field dynamics

Andrew D. Bragg^{1,†} and Stephen M. de Bruyn Kops²

¹Department of Civil and Environmental Engineering, Duke University, Durham, NC 27708, USA

²Department of Mechanical and Industrial Engineering, University of Massachusetts Amherst, Amherst, MA 01003, USA

(Received 1 August 2023; revised 21 May 2024; accepted 21 May 2024)

Recently, direct numerical simulations (DNS) of stably stratified turbulence have shown that as the Prandtl number (Pr) is increased from 1 to 7, the mean turbulent potential energy dissipation rate (TPE-DR) drops dramatically, while the mean turbulent kinetic energy dissipation rate (TKE-DR) increases significantly. Through an analysis of the equations governing the fluctuating velocity and density gradients we provide a mechanistic explanation for this surprising behaviour and test the predictions using DNS. We show that the mean density gradient gives rise to a mechanism that opposes the production of fluctuating density gradients, and this is connected to the emergence of ramp cliffs. The same term appears in the velocity gradient equation but with the opposite sign, and is the contribution from buoyancy. This term is ultimately the reason why the TPE-DR reduces while the TKE-DR increases with increasing Pr . Our analysis also predicts that the effects of buoyancy on the smallest scales of the flow become stronger as Pr is increased, and this is confirmed by our DNS data. A consequence of this is that the standard buoyancy Reynolds number does not correctly estimate the impact of buoyancy at the smallest scales when Pr deviates from 1, and we derive a suitable alternative parameter. Finally, an analysis of the filtered gradient equations reveals that the mean density gradient term changes sign at sufficiently large scales, such that buoyancy acts as a source for velocity gradients at small scales, but as a sink at large scales.

Key words: stratified turbulence, turbulence theory

† Email address for correspondence: andrew.bragg@duke.edu

1. Introduction

In simple fluids where molecular transport is modelled as a gradient-diffusion process, the mixing rates of quantities such as momentum, heat and species are determined by the associated molecular diffusion coefficient and the magnitude of spatial gradients of the quantity. In a turbulent flow, complex stirring motions lead to the intensification of spatial gradients of flow quantities, which in turn enhances the mixing rates. In this sense, the mixing rates are controlled by the stirring processes themselves. This fact is often exploited when modelling mixing rates because the wide range of dynamically relevant length and time scales in high Reynolds number turbulent flows means that the small-scale mixing often cannot be directly resolved, and so it is instead modelled indirectly based on stirring rates at resolved scales. This assumption underlies large eddy simulations which model the unresolved small-scale mixing by connecting it to the resolved large-scale dynamics. The assumption also underlies the classical k - ϵ closure (where k is the turbulent kinetic energy, and ϵ is the turbulent kinetic energy dissipation rate) for the Reynolds averaged Navier Stokes equations (RANS), as well as models based on a turbulent Prandtl number (we do not distinguish between heat and species and use the term Prandtl number for both). In particular, typical RANS models carry information primarily about the large-scale dynamics. On the other hand, ϵ is primarily associated with small-scale physical processes, and the strategy in all RANS models is to model ϵ indirectly through its connection to the large-scale energetics via the energy cascade. Second-order closures for RANS and conditional moment closure are examples of approaches that do not directly couple mixing and stirring rates, however, nevertheless, the former is inferred from the latter without information about the dynamics at the smallest scales where the mixing actually takes place.

The motivation for the research reported here is that in stably stratified flows (subject to the Boussinesq approximation), varying the diffusion coefficient of the scalar has been observed to affect the mixing rates of not only the scalar but also of momentum. In the very simple configuration of initially homogeneous and isotropic turbulence subjected to a stabilizing density gradient, Riley, Couchman & de Bruyn Kops (2023) find that not only is the dissipation rate of potential energy significantly lower at Prandtl number $Pr = 7$ than at $Pr = 1$, but the dissipation rate of kinetic energy is also higher at $Pr = 7$. In fact, it has been known for some time that higher Pr results in slower mixing of heat in stratified flows (Smyth, Moum & Caldwell 2001). More recently, Salehipour & Peltier (2015) found that Pr has a strong effect on secondary instabilities in stratified flows, and Legaspi & Waite (2020) observed transfer of potential to kinetic energy at small scales that depends on Pr .

An interesting feature of the homogeneous flow studied by Riley *et al.* (2023) is that the large-scale structures are not obviously affected by the changes in Pr other than that they lose energy at differing rates depending on Pr . But if mixing rates are determined by stirring rates, then since the mixing rates were observed in Riley *et al.* (2023) to depend strongly on Pr , the stirring rates at some scales in the flow must also be strongly affected by Pr . The connection between stirring and mixing rates in stratified turbulence has been traditionally approached from the perspective of multiscale flow energetics, i.e. analysing kinetic and potential energies using Fourier analysis. However, to understand the physical mechanism by which stirring and mixing rates in stratified turbulence are affected by Pr , we find it more insightful to study the problem by analysing the equations governing velocity and scalar gradients in the flow. Production mechanisms in these equations are associated with the stirring processes that intensify flow gradients, and the magnitude of the resulting gradients determines the mixing rates.

In the context of homogeneous, isotropic turbulence, studying turbulent flows from the perspective of velocity gradient dynamics has a long and rich history that has led to numerous insights into the physics of small-scale turbulence (Vieillefosse 1982; Ashurst *et al.* 1987; Nomura & Post 1998; Chertkov, Pumir & Shraiman 1999; Tsinober 2001; Chevillard & Meneveau 2006; Gulitski *et al.* 2007; Meneveau 2011; Danish & Meneveau 2018; Carbone, Iovieno & Bragg 2020; Tom, Carbone & Bragg 2021). For stratified flows where the momentum and density fields are coupled, velocity gradient dynamics would need to be studied in conjunction with that of density gradients, and very little has been done on this. Diamessis & Nomura (2000) studied the interaction of vorticity, strain-rate and density gradient fields in stratified homogeneous sheared turbulence. Through the buoyancy force, density gradients give rise to a baroclinic torque term in the vorticity equation, and they argued that the interaction of vorticity and density gradients involves an inherent negative feedback between baroclinic torque and reorientation of the density gradients by the vorticity. By contrast, the interaction of the strain-rate and density gradient fields involves a positive feedback that promotes the persistence of vertical density gradients. The stratified flows in their study exhibited a decay of turbulent kinetic energy, and as time advanced, the third invariant of the velocity gradient tensor approached zero, indicating that the flow was becoming dynamically two-dimensional. More recent studies are the insightful studies of Sujovolsky, Mindlin & Mininni (2019), Sujovolsky & Mininni (2020) and Marino *et al.* (2022). In these, simplified forms of the velocity and density gradient equations were considered in which molecular transport and the non-local pressure Hessian terms were discarded (similar in spirit to the restricted Euler model of Vieillefosse 1982). For the resulting simplified model, invariant manifolds were discovered, and the way that phase-space trajectories move between these manifolds was shown to explain the enhanced intermittency and marginal instability that has been observed in stably stratified flows when the Froude number is within a certain range (Rorai, Mininni & Pouquet 2014; Feraco *et al.* 2018).

In our study we will analyse the exact (within the Boussinesq framework) forms of the coupled velocity and density gradient equations in order to understand the mechanism responsible for the strong Pr dependence of mixing rates in stably stratified turbulence observed in Riley *et al.* (2023). It will be shown that the mechanism is associated with the competition between distinct production terms in the gradient equations that are associated with either the fluctuating or mean density gradient field. The term associated with the mean density gradient actually opposes the production of fluctuating density gradients, and this is ultimately the effect responsible for the momentum mixing rate increasing and the density mixing rate decreasing as Pr is increased, as observed in Riley *et al.* (2023). Furthermore, we also study the behaviour of velocity and passive scalar gradients in the context of stationary, homogeneous, isotropic turbulence with a mean-scalar gradient. It will be seen that the mechanism responsible for the striking effect of Pr on scalar mixing rates in stratified turbulence is in fact already present even in the case of a passive scalar. It is simply that this mechanism plays a very small role in the passive scalar case, although it could play an important role even in that case depending upon the parameter regime of the flow.

2. Theory: gradient dynamics for high Reynolds number neutral flows

So that we can consider passive and active scalars using the same notation, let the scalar in all cases be density ρ and we assume the non-hydrostatic Boussinesq approximation. Then $\rho = \rho_r + \gamma z + \varrho$, where ρ_r is the reference density, and ϱ is the fluctuation about the mean density $\langle \rho \rangle = \rho_r + \gamma z$, with γ a constant. Furthermore, it is convenient to introduce the

variable $\phi \equiv \rho g / (N \rho_r)$ which has dimensions of a velocity, where g is the gravitational acceleration and where $N \equiv \sqrt{-g\gamma/\rho_r}$ is the buoyancy frequency. The equations for the velocity \mathbf{u} and ϕ are

$$D_t \mathbf{u} = -\nabla p + \nu \nabla^2 \mathbf{u} - N \phi \mathbf{e}_z + \mathbf{F}, \tag{2.1}$$

$$D_t \phi = (\nu/Pr) \nabla^2 \phi + N u_z, \tag{2.2}$$

where $D_t \equiv \partial_t + (\mathbf{u} \cdot \nabla)$ is the Lagrangian derivative, p is the pressure, ν is the kinematic viscosity, \mathbf{e}_z is the unit vector in the vertical direction, \mathbf{F} is a forcing term and Pr is the Prandtl number.

For statistically homogeneous flows (as considered in this paper), the equations governing the average kinetic energy (per unit mass) $\langle \|\mathbf{u}\|^2 \rangle / 2$ and average ‘scalar energy’ $\langle \phi^2 \rangle / 2$ are

$$(1/2) \partial_t \langle \|\mathbf{u}\|^2 \rangle = -2\nu \langle \|\mathbf{S}\|^2 \rangle - N \langle \phi u_z \rangle + \langle \mathbf{F} \cdot \mathbf{u} \rangle, \tag{2.3}$$

$$(1/2) \partial_t \langle \phi^2 \rangle = -(\nu/Pr) \langle \|\mathbf{B}\|^2 \rangle + N \langle \phi u_z \rangle, \tag{2.4}$$

where $\mathbf{S} \equiv (\mathbf{A} + \mathbf{A}^\top) / 2$ is the strain-rate tensor, $\mathbf{A} \equiv \nabla \mathbf{u}$ and $\mathbf{B} \equiv \nabla \phi$. Here and throughout, $\|\cdot\|$ denotes a Frobenius norm, and $\langle \cdot \rangle$ denotes an ensemble average (which is approximated in the direct numerical simulation (DNS) results using appropriate combinations of spatial and temporal averages).

In (2.3) and (2.4), the energy dissipation rates are $\langle \epsilon \rangle \equiv 2\nu \langle \|\mathbf{S}\|^2 \rangle$ and $\langle \chi \rangle \equiv (\nu/Pr) \langle \|\mathbf{B}\|^2 \rangle$. In the context of stratified flows, $\langle \phi^2 \rangle / 2$ can be interpreted as the mean turbulent potential energy in the flow and $\langle \chi \rangle$ is its dissipation rate. One of the key goals of this work is to understand the mechanisms controlling $\langle \epsilon \rangle$ and $\langle \chi \rangle$ and how they depend upon Pr . Since these dissipation rates are fundamentally related to the gradient fields \mathbf{S} and \mathbf{B} , it is the behaviour of these gradients that must be understood in order to understand the dissipation rates and their dependence on Pr .

Derived from (2.1) and (2.2), the equations governing \mathbf{S} and \mathbf{B} are

$$D_t \mathbf{S} = -\mathbf{S} \cdot \mathbf{S} - (1/4)(\boldsymbol{\omega} \boldsymbol{\omega} - \|\boldsymbol{\omega}\|^2 \mathbf{I}) - \nabla \nabla p + \nu \nabla^2 \mathbf{S} - (N/2)(\mathbf{B} \mathbf{e}_z + \mathbf{e}_z \mathbf{B}) + \nabla \mathbf{F}_S, \tag{2.5}$$

$$D_t \mathbf{B} = -\mathbf{A}^\top \cdot \mathbf{B} + (\nu/Pr) \nabla^2 \mathbf{B} + N \mathbf{A}^\top \cdot \mathbf{e}_z, \tag{2.6}$$

where $\nabla \mathbf{F}_S \equiv (1/2)(\nabla \mathbf{F} + \nabla \mathbf{F}^\top)$, and the role of each of the terms in these equations will be discussed in the analysis that follows.

Of particular importance to the analysis in this paper is the competition between the nonlinear/bi-linear terms in these equations and the terms involving the mean-scalar gradient. To assess this, we can consider the scaling of these terms. To scale \mathbf{S} we use $\sigma_S \equiv \sqrt{\langle \|\mathbf{S}\|^2 \rangle}$, to scale $\boldsymbol{\omega}$ we use $\sigma_\omega \equiv \sqrt{\langle \|\boldsymbol{\omega}\|^2 \rangle}$ and using the results of Betchov (1956) we have $\sigma_\omega = \sqrt{2} \sigma_S = \sigma_A$, where $\sigma_A \equiv \sqrt{\langle \|\mathbf{A}\|^2 \rangle}$. Due to the pressure Poisson equation, the pressure Hessian $\nabla \nabla p$ is scaled by σ_S^2 , and to scale \mathbf{B} we use $\sigma_B \equiv \sqrt{\langle \|\mathbf{B}\|^2 \rangle}$. With these choices we have

$$\frac{\| - (N/2)(\mathbf{B} \mathbf{e}_z + \mathbf{e}_z \mathbf{B}) \|}{\| -\mathbf{S} \cdot \mathbf{S} - (1/4)(\boldsymbol{\omega} \boldsymbol{\omega} - \|\boldsymbol{\omega}\|^2 \mathbf{I}) - \nabla \nabla p \|} \sim O(\Lambda_S), \tag{2.7}$$

$$\frac{\| N \mathbf{A}^\top \cdot \mathbf{e}_z \|}{\| -\mathbf{A}^\top \cdot \mathbf{B} \|} \sim O(\Lambda_B), \tag{2.8}$$

where $\Lambda_S \equiv N \sigma_B / \sigma_S^2$, and $\Lambda_B \equiv N / \sigma_B$.

The parameter Λ_S is essentially an inverse small-scale Froude number since it comes from the ratio of the size of the buoyancy gradient to the size of the nonlinear term in the equation for \mathbf{S} . We will return later to consider the meaning of Λ_S and its relation to more familiar parameters in stratified turbulence. In the limit $\Lambda_S \rightarrow 0$ the contribution from buoyancy to the dynamics of \mathbf{S} vanishes since the equation is regular in this limit, and this corresponds to the passive scalar limit.

The parameter Λ_B (which is effectively equal to the inverse of the square root of the Cox number that is used in Salehipour & Peltier 2015) determines the importance of the mean-scalar gradient on the evolution of \mathbf{B} , and this parameter will be seen to be important for understanding the strong effect of Pr on the turbulent kinetic energy (TKE) and turbulent potential energy (TPE) dissipation rates in stratified turbulence. Although $\Lambda_B \equiv N/\sigma_B$ explicitly depends on N , since the equation for \mathbf{B} is linear, then for the passive scalar limit where \mathbf{u} and hence \mathbf{A} is independent of N , the dependence of Λ_B on N vanishes. To show this, we write the equation for \mathbf{B} in operator form as $\mathcal{L}\{\mathbf{B}\} = N\mathbf{A}^\top \cdot \mathbf{e}_z$, where the linear operator is $\mathcal{L}\{\cdot\} \equiv D_t - (\nu/Pr)\nabla^2 + \mathbf{A}^\top \cdot$. Since the inverse of a linear operator is also linear, we have $\mathbf{B} = \mathcal{L}^{-1}\{N\mathbf{A}^\top \cdot \mathbf{e}_z\} = N\mathcal{L}^{-1}\{\mathbf{A}^\top \cdot \mathbf{e}_z\}$. From this, it follows that

$$\sigma_B = N\sqrt{\langle \|\mathcal{L}^{-1}\{\mathbf{A}^\top \cdot \mathbf{e}_z\}\|^2 \rangle}, \tag{2.9}$$

and hence $\Lambda_B \equiv N/\sigma_B$ is independent of N for a passive scalar (except for the trivial requirement that $N \neq 0$ since the scalar is driven by a mean-scalar gradient). The size of Λ_B is therefore controlled only by the parameter ν/Pr in the passive scalar limit.

In what follows, we will begin by considering the dynamics of neutrally buoyant flows corresponding to the case for which the scalar is passive, since it will be shown that some of the key properties of a passive scalar driven by a mean-scalar gradient play an important role in the behaviour of stratified flows. For the passive scalar case it will be assumed that the forcing \mathbf{F} generates a statistically stationary, isotropic turbulent flow. We will also consider the case where the scalars are introduced into a fully developed turbulent flow with $\mathbf{B}(0) = \mathbf{0}$ since this is the situation that will be considered later in the DNS of decaying stratified turbulence, and we want to understand how \mathbf{B} evolves from its initial state to its quasi-stationary behaviour. Note that for the passive scalar case the statistics of \mathbf{B} change trivially under the transformation $\gamma \rightarrow -\gamma$, and so, for consistency with the stably stratified case, we only consider $\gamma < 0$ in the analysis that follows such that $N \in \mathbb{R}^+$.

2.1. Impact of the Batchelor regime

When $Pr \neq 1$ there is a difference between the smallest scales of the momentum and scalar fields. While the smallest scale (in a mean-field sense) of the momentum field is the Kolmogorov scale η , the smallest scale of the scalar field is the Batchelor scale $\eta_B = Pr^{-1/2}\eta$ when $Pr \geq 1$ (Batchelor 1959), while for $Pr < 1$ it is the Obukhov–Corrsin scale $\eta_{OC} = Pr^{-3/4}\eta$ (Obukhov 1949; Corrsin 1951). When $Pr \gg 1$, there is a separation of scales $\eta \gg \eta_B$ corresponding to the so-called ‘viscous–convective range’ in which the effects of viscosity are important, but the effects of molecular diffusion on the scalar field are not. In terms of (2.6), the significance of this is that for the term $-\mathbf{A}^\top \cdot \mathbf{B}$, which describes how the fluctuating velocity gradients amplify (or suppress) the fluctuating scalar gradients (as well as re-orientating them), \mathbf{A} and \mathbf{B} may exhibit fluctuations at different scales in the flow. When $Pr \gg 1$, \mathbf{B} will exhibit fluctuations on a much finer scale than \mathbf{A} , on average, and this ‘de-localization’ between the scale at which \mathbf{A} and \mathbf{B}

fluctuate impacts the behaviour of $-\mathbf{A}^\top \cdot \mathbf{B}$. This de-localization effect was previously considered in Nazarenko & Laval (2000) for passive scalars in two-dimensional turbulence using Fourier analysis, rather than the gradient fields as discussed here.

The de-localization effect and the associated Batchelor scaling that arises in the viscous–convective regime can impact the Pr dependence of $\langle \chi \rangle$. In Donzis, Sreenivasan & Yeung (2005), a model for $\langle \chi \rangle$ was presented that captures this effect. In particular, for the case of $Pr \geq 1$, the scalar spectrum in the inertial–convective range (where the effects of ν and Pr are both assumed to be unimportant) was modelled using a Obukhov–Corrsin spectrum (Obukhov 1949; Corrsin 1951), and that in the viscous–convective range was modelled using a Batchelor spectrum, leading to

$$\frac{L \langle \chi \rangle}{U \langle \phi^2 \rangle} \sim \frac{1}{c_1(f^{2/3} - c_3 Re_\lambda^{-1}) + c_2 Re_\lambda^{-1} \ln Pr}, \quad (2.10)$$

where L is the integral length scale of the velocity field, U is the root-mean-square (r.m.s.) velocity, Re_λ is the Taylor Reynolds number, $f \equiv A(1 + \sqrt{1 + (B/Re_\lambda)^2})$ and $A \approx 0.2$, $B \approx 92$, $c_1 \approx 0.6$, $c_2 \approx (5/3)\sqrt{15}$, $c_3 \approx \sqrt{15}$. These values were determined by fitting the model to DNS data (since the assumed spectra involve unknown $O(1)$ coefficients), except for the factors involving $\sqrt{15}$, which arise due to isotropy of the flow.

The $\ln Pr$ dependence in (2.10) arises from the contribution due to the Batchelor spectrum for the viscous–convective range. This model predicts that for finite Pr , $\lim_{Re_\lambda \rightarrow \infty} [L\langle \chi \rangle / (U\langle \phi^2 \rangle)] \sim 1/(c_1 2^{2/3} A^{2/3})$, i.e. a constant reflecting anomalous behaviour in this limit. However, for finite Re_λ it predicts $\lim_{Pr \rightarrow \infty} [L\langle \chi \rangle / (U\langle \phi^2 \rangle)] \sim Re_\lambda / (c_2 \ln Pr)$, i.e. no dissipation anomaly. This logarithmic behaviour was confirmed in Donzis *et al.* (2005) at low Re_λ , and more recently in Buaria *et al.* (2021b) at a higher Reynolds number $Re_\lambda = 140$ over the range $Pr \in [1, 512]$. In view of the derivation of (2.10), the interpretation is that the behaviour of $L\langle \chi \rangle / (U\langle \phi^2 \rangle)$ will only be anomalous when the Batchelor regime makes a sub-leading contribution to $L\langle \chi \rangle / (U\langle \phi^2 \rangle)$, and the Obukhov–Corrsin regime dominates.

In addition to the model in (2.10), Donzis *et al.* (2005) also derived a model for $L\langle \chi \rangle / (U\langle \phi^2 \rangle)$ that applies for $Pr < 1$ by integrating the Obukhov–Corrsin spectrum up to the cutoff wavenumber $k \sim 1/\eta_{OC}$. This model also predicts a Pr dependence of $L\langle \chi \rangle / (U\langle \phi^2 \rangle)$, however, in this case it involves $Pr^{1/2}$ rather than the $\ln Pr$ factor that arises for $Pr \geq 1$. The Pr dependence of $L\langle \chi \rangle / (U\langle \phi^2 \rangle)$ only vanishes in the regime $Pr < 1$ when $Re_\lambda Pr^{1/2}$ is sufficiently large.

2.2. Behaviour of production terms and the role of ramp-cliff structures

In addition to the de-localization effect that influences the behaviour of $-\mathbf{A}^\top \cdot \mathbf{B}$ in (2.6) when $Pr > 1$, there is a second way in which Pr can influence the stirring processes that govern the amplification of \mathbf{B} , which in turn can influence the Pr dependence of $\langle \chi \rangle$. This second effect arises due to a Pr -dependent competition between $-\mathbf{A}^\top \cdot \mathbf{B}$ and $N\mathbf{A}^\top \cdot \mathbf{e}_z$ in (2.6). This effect was not accounted for in the model of Donzis *et al.* (2005) for $\langle \chi \rangle$ because they assumed that the direct effect of the mean-scalar gradient is unimportant for the behaviour of $\langle \chi \rangle$. Provided that $Re_\lambda \gg 1$ and $Pr \geq O(1)$, we expect $\Lambda_B \ll 1$, reflecting that the fluctuating scalar gradients are much larger than the mean density gradient. As a result, this second effect is usually not important for passive scalars in turbulent flows. Nevertheless, we explain it in significant detail here because it will be shown that it is in

fact the main contributor to the strong Pr dependence of $\langle \chi \rangle$ observed for stratified flows in Riley *et al.* (2023). This therefore provides mechanistic insights into how scalar mixing can differ in significant ways for neutral and stratified flows.

From (2.6) we obtain

$$\frac{1}{2}D_t\|\mathbf{B}\|^2 = \mathcal{P}_{B1} + \mathcal{P}_{B2} + (\nu/Pr)\nabla^2\|\mathbf{B}\|^2 - \mathcal{D}_B, \quad (2.11)$$

where

$$\mathcal{P}_{B1} \equiv -\mathbf{B} \cdot \mathbf{A}^\top \cdot \mathbf{B}, \quad (2.12)$$

is the production term associated with the fluctuating scalar gradient

$$\mathcal{P}_{B2} \equiv N\mathbf{B} \cdot \mathbf{A}^\top \cdot \mathbf{e}_z, \quad (2.13)$$

is the production term associated with the mean scalar gradient and $\mathcal{D}_B \equiv (\nu/Pr)\|\nabla\mathbf{B}\|^2$ is the dissipation rate of $\|\mathbf{B}\|^2$.

For a statistically homogeneous flow

$$\frac{1}{2}\partial_t\langle\|\mathbf{B}\|^2\rangle = \langle\mathcal{P}_{B1}\rangle + \langle\mathcal{P}_{B2}\rangle - \langle\mathcal{D}_B\rangle. \quad (2.14)$$

Unlike the dissipation term $\langle\mathcal{D}_B\rangle$, the production terms $\langle\mathcal{P}_{B1}\rangle$ and $\langle\mathcal{P}_{B2}\rangle$ are not sign definite and so may in fact act to oppose the growth of $\langle\|\mathbf{B}\|^2\rangle$ (despite the misnomer, we refer to them as production terms in keeping with the standard terminology used for the production terms in the Reynolds stress equation that are also not sign definite Pope 2000). We must therefore consider the sign of these terms in order to understand the role they play in governing $\langle\|\mathbf{B}\|^2\rangle$. It will be shown that the sign of $\langle\mathcal{P}_{B2}\rangle$ is intimately connected to the emergence of ramp-cliff structures in the scalar field, and we therefore first consider in view of (2.6) how these structures form, and then show how this impacts the sign of $\langle\mathcal{P}_{B2}\rangle$ relative to that of $\langle\mathcal{P}_{B1}\rangle$.

When a scalar field is driven by a mean scalar gradient, ramp-cliff structures emerge which are associated with the fluctuating gradients developing a skewness whose sign corresponds to the direction of the imposed mean-scalar gradient (Holzer & Siggia 1994; Sreenivasan 2018; Buaria *et al.* 2021a). To understand how this asymmetry arises from the equation for \mathbf{B} , we may consider the case where the probability density function (p.d.f.) of the initial condition $\mathbf{B}(0)$ is an isotropic and symmetric function, and uncorrelated from \mathbf{A} . Writing \mathbf{B} in terms of Cartesian components, the equation for $B_z \equiv \mathbf{B} \cdot \mathbf{e}_z$ is obtained from (2.6)

$$D_t B_z = -B_x A_{xz} - B_y A_{yz} - (B_z - N)A_{zz} + (\nu/Pr)\nabla^2 B_z, \quad (2.15)$$

where subscripts x and y denote components in the horizontal directions of the flow. For an isotropic flow, the p.d.f.s of A_{xz} and A_{yz} are symmetric. Therefore, given the symmetric initial condition for \mathbf{B} , the symmetry breaking responsible for the p.d.f. of B_z becoming skewed cannot come from the terms $-B_x A_{xz} - B_y A_{yz}$ (or $\nabla^2 B_z$), but must come from $-(B_z - N)A_{zz}$. The strongest symmetry breaking associated with this term is generated in the range $|B_z| \in [0, N)$ and so we focus on this range. In the range $|B_z| \in [0, N)$ we can write $-(B_z - N)A_{zz} = |B_z - N|A_{zz}$, and so $A_{zz} < 0$ events drive B_z towards negative values, while $A_{zz} > 0$ events drive B_z towards positive values. Since in an isotropic flow, the p.d.f. of A_{zz} is negatively skewed, then the term $|B_z - N|A_{zz}$ will generate larger negative values of B_z than positive ones, and hence negative skewness. If the flow field were Gaussian, however, this mechanism would be absent. Nevertheless, random Gaussian flows also generate skewed p.d.f.s for B_z (Holzer & Siggia 1994) and, therefore, there must be another mechanism responsible for this. This second mechanism arises from the fact

that, starting from the isotropic initial condition for $B_z(0)$ and in a flow where the p.d.f. of A_{zz} is symmetric, statistically $-(B_z(0) - N)A_{zz}$ will be larger in regions where $B_z(0) < 0$ than in regions where $B_z(0) > 0$. This means that $-(B_z(0) - N)A_{zz}$ will generate larger negative values of B_z than positive ones, and hence negative skewness. This mechanism fundamentally arises in (2.6) due to the ability of the fluctuating production $-\mathbf{A}^\top \cdot \mathbf{B}$ and mean gradient production $N\mathbf{A}^\top \cdot \mathbf{e}_z$ terms to act together or against each other, and skewness of the p.d.f. will be generated in the direction for which the two terms act together. The same argument applied to the case $\gamma > 0$ shows that in this case, B_z will be positively skewed, the opposite of the $\gamma < 0$ case.

In view of this, the emergence of ramp-cliff structures is determined by the interplay between $-\mathbf{A}^\top \cdot \mathbf{B}$ and $N\mathbf{A}^\top \cdot \mathbf{e}_z$, which are associated with the production terms \mathcal{P}_{B1} and \mathcal{P}_{B2} in (2.11). It may therefore be anticipated that ramp-cliff structures are also relevant to understanding the signs of the average terms $\langle \mathcal{P}_{B1} \rangle$ and $\langle \mathcal{P}_{B2} \rangle$. To consider this, we begin by examining the behaviour of $\langle \mathcal{P}_{B1} \rangle$ and $\langle \mathcal{P}_{B2} \rangle$ in the ‘short-time regime’ for the case where scalars are introduced to a fully developed turbulent flow with initial condition $\mathbf{B}(x, 0) = \mathbf{0} \forall x$ (a situation that will be of relevance to the DNS shown later). Using the Kolmogorov time scale τ_η , for $t \ll \tau_\eta$ we have $\tau_\eta \mathbf{A}(t) = \tau_\eta \mathbf{A}(0) + O(t/\tau_\eta)$, and inserting this into (2.6) yields the solution $\tau_\eta \mathbf{B}(t) \sim \tau_\eta N t \mathbf{A}^\top(0) \cdot \mathbf{e}_z + O([t/\tau_\eta]^2)$ when $\mathbf{B}(0) = \mathbf{0}$. From this we obtain for $t \ll \tau_\eta$

$$\langle \mathcal{P}_{B2} \rangle \sim N^2 t \langle \|\mathbf{A}^\top(0) \cdot \mathbf{e}_z\|^2 \rangle, \tag{2.16}$$

and hence at short times $\langle \mathcal{P}_{B2} \rangle > 0$. Using the same approach we can also derive

$$\langle \mathcal{P}_{B1} \rangle \sim N^2 t^2 \langle \mathcal{P}_{A1} \rangle. \tag{2.17}$$

The invariant

$$\mathcal{P}_{A1} \equiv -\mathbf{A}^\top : (\mathbf{A} \cdot \mathbf{A}), \tag{2.18}$$

is the velocity gradient self-amplification term and it is positive on average (Tsinober 2000) so that it acts as a source term in the equation for $\partial_t \langle \|\mathbf{A}\|^2 \rangle$. As a result $\langle \mathcal{P}_{B1} \rangle > 0$ at short times, but its contribution is sub-leading compared with that from the mean gradient production term $\langle \mathcal{P}_{B2} \rangle$.

The question is whether the sign of these production terms remains the same once the stationary regime $\partial_t \langle \|\mathbf{B}\|^2 \rangle = 0$ has been attained where the ramp-cliff structures are fully developed. The production terms may be re-expressed using $\mathbf{B} = \|\mathbf{B}\| \mathbf{e}_B$ and index notation as

$$\langle \mathcal{P}_{B1} \rangle = -\langle \|\mathbf{B}\|^2 (\mathbf{e}_B \cdot \mathbf{e}_j) A_{ji} (\mathbf{e}_i \cdot \mathbf{e}_B) \rangle, \tag{2.19}$$

$$\langle \mathcal{P}_{B2} \rangle = N \langle \|\mathbf{B}\| (\mathbf{e}_B \cdot \mathbf{e}_j) A_{ji} (\mathbf{e}_i \cdot \mathbf{e}_z) \rangle, \tag{2.20}$$

where \mathbf{e}_i are the basis vectors for the Cartesian coordinate system, with $i, j \in \{x, y, z\}$. Written in this form it is clear that these terms will only have the same sign if $\mathbf{e}_i \cdot \mathbf{e}_B$ and $\mathbf{e}_i \cdot \mathbf{e}_z$ tend to have opposite signs (since we are considering $N > 0$). This, in turn, depends on the alignments of \mathbf{e}_B and \mathbf{e}_z , which are connected to the formation of the ramp-cliff structures in the flow.

Since $\langle \phi \rangle = 0$ then $\langle B_z \rangle = 0$, because $\langle B_z \rangle = \langle \nabla_z \phi \rangle = \nabla_z \langle \phi \rangle = 0$. Ramp-cliff structures are associated with B_z having larger negative than positive values (when $\gamma < 0$), such that the odd moments of B_z are negative. However, in order for $\langle B_z \rangle = 0$ to be satisfied, it must be the case that events where $B_z > 0$ are more probable than those with $B_z < 0$. Since $B_z = \|\mathbf{B}\| \mathbf{e}_B \cdot \mathbf{e}_z$, a higher probability of $B_z > 0$ events corresponds

to a higher probability of $\mathbf{e}_B \cdot \mathbf{e}_z > 0$ events than $\mathbf{e}_B \cdot \mathbf{e}_z < 0$ events. Due to this, the most probable configuration is that the signs of $\mathbf{e}_i \cdot \mathbf{e}_z$ and $\mathbf{e}_i \cdot \mathbf{e}_B$ will be the same, and therefore once ramp-cliff structures emerge in the field, the production terms $\langle \mathcal{P}_{B1} \rangle$ and $\langle \mathcal{P}_{B2} \rangle$ will have opposite signs.

This argument establishes that $\langle \mathcal{P}_{B1} \rangle$ and $\langle \mathcal{P}_{B2} \rangle$ will have opposite signs once ramp-cliff structures in the flow have developed. The argument does not depend on how strong the ramp-cliff structures are, but only that they exist, such that the probability distribution of $\mathbf{e}_B \cdot \mathbf{e}_z$ is not strictly uniform. Therefore, although the ramp-cliff structures for a passive scalar are known to weaken as Pr is increased beyond $Pr = 1$, with the skewness of B_z asymptotically approaching zero in the limit $Pr \rightarrow \infty$ (Buaria *et al.* 2021a; Shete *et al.* 2022), $\langle \mathcal{P}_{B1} \rangle$ and $\langle \mathcal{P}_{B2} \rangle$ will have opposite signs at all finite Pr . The argument given above does not, however, establish the sign of $\langle \mathcal{P}_{B2} \rangle$, but only that its sign must be opposite to that of $\langle \mathcal{P}_{B1} \rangle$. To determine the sign of $\langle \mathcal{P}_{B2} \rangle$ we would also have to consider the behaviour of $\|\mathbf{B}\|$ and A_{ji} in the expression $\langle \mathcal{P}_{B2} \rangle = N \langle \|\mathbf{B}\| (\mathbf{e}_B \cdot \mathbf{e}_j) A_{ji} (\mathbf{e}_i \cdot \mathbf{e}_z) \rangle$. We can, however, infer its sign by the following argument: in order for the stationary regime $\partial_t \langle \|\mathbf{B}\|^2 \rangle = 0$ to be sustained, it must be that case that $\langle \mathcal{P}_{B1} \rangle + \langle \mathcal{P}_{B2} \rangle > 0$. If $\Lambda_B < 1$, then according to the scaling introduced in § 2, $|\langle \mathcal{P}_{B1} \rangle| > |\langle \mathcal{P}_{B2} \rangle|$, and it therefore follows from the argument above that we must have $\langle \mathcal{P}_{B1} \rangle > 0$ and $\langle \mathcal{P}_{B2} \rangle < 0$ in the stationary regime due to the ramp-cliff structures.

2.3. The importance of the mean-scalar gradient production

Since $\langle \mathcal{P}_{B2} \rangle < 0$, then the mean-scalar gradient term $\langle \mathcal{P}_{B2} \rangle$ acts to oppose the growth of $\langle \|\mathbf{B}\|^2 \rangle$, and hence acts to decrease the scalar dissipation rate $\langle \chi \rangle$. In the passive scalar limit, high Reynolds number turbulent flows with $Pr \geq O(1)$ will exist in the regime $\Lambda_B \ll 1$ due to the fluctuating scalar gradients being much larger than the mean scalar gradient. Therefore, the effect of $\langle \mathcal{P}_{B2} \rangle$ on $\langle \chi \rangle$ is expected to be negligible in the high Reynolds number passive scalar regime where $|\langle \mathcal{P}_{B2} \rangle|/|\langle \mathcal{P}_{B1} \rangle| \sim O(\Lambda_B) \ll 1$, which we will later confirm with DNS data.

The mean-scalar gradient term must nevertheless play a crucial implicit role because without it the fluctuating scalar gradients would decay. To see this more clearly we should consider the behaviour of the filtered gradients which provide information about the scalar gradients at different scales.

We define the filtering operation for an arbitrary field quantity Y to be

$$\tilde{Y}(\mathbf{x}, t) \equiv \int_{\mathbb{R}^3} \mathcal{G}_\ell(\|\mathbf{x} - \mathbf{x}'\|) Y(\mathbf{x}', t) d\mathbf{x}', \quad (2.21)$$

where \mathcal{G}_ℓ is an isotropic filter kernel with filtering length scale ℓ (the particular choice of kernel, e.g. a Gaussian or box function, is not important here). Applying this filtering operator to (2.2) and taking the gradient of the resulting equation leads to

$$\tilde{D}_t \tilde{\mathbf{B}} = -\tilde{\mathbf{A}}^\top \cdot \tilde{\mathbf{B}} + (\nu/Pr) \nabla^2 \tilde{\mathbf{B}} + N \tilde{\mathbf{A}}^\top \cdot \mathbf{e}_z - \nabla \nabla \cdot \boldsymbol{\tau}_\phi, \quad (2.22)$$

where $\tilde{D}_t \equiv \partial_t + (\tilde{\mathbf{u}} \cdot \nabla)$, and $\boldsymbol{\tau}_\phi \equiv \tilde{\mathbf{u}}\tilde{\phi} - \tilde{\mathbf{u}}\tilde{\phi}$ is the sub-grid stress vector.

From (2.22), the equation governing $\partial_t \langle \|\tilde{\mathbf{B}}\|^2 \rangle$ can be constructed, and for a statistically stationary, homogeneous flow it reduces to

$$0 = -\langle \tilde{\mathbf{B}} \cdot \tilde{\mathbf{A}}^\top \cdot \tilde{\mathbf{B}} \rangle - (\nu/Pr) \langle \|\nabla \tilde{\mathbf{B}}\|^2 \rangle + N \langle \tilde{\mathbf{B}} \cdot \tilde{\mathbf{A}}^\top \cdot \mathbf{e}_z \rangle - \langle \tilde{\mathbf{B}} \cdot \nabla \nabla \cdot \boldsymbol{\tau}_\phi \rangle. \quad (2.23)$$

For $\ell \gg \eta_B$, where η_B is the Batchelor length scale, the dissipation term $(\nu/Pr) \langle \|\nabla \tilde{\mathbf{B}}\|^2 \rangle$ can be ignored because almost all of the scalar dissipation takes place at scales $\ell = O(\eta_B)$.

Therefore, for $\ell \gg \eta_B$ we have the balance

$$-\langle \tilde{\mathbf{B}} \cdot \tilde{\mathbf{A}}^\top \cdot \tilde{\mathbf{B}} \rangle + N \langle \tilde{\mathbf{B}} \cdot \tilde{\mathbf{A}}^\top \cdot \mathbf{e}_z \rangle \sim \langle \tilde{\mathbf{B}} \cdot \nabla \nabla \cdot \boldsymbol{\tau}_\phi \rangle. \quad (2.24)$$

The term $\langle \tilde{\mathbf{B}} \cdot \nabla \nabla \cdot \boldsymbol{\tau}_\phi \rangle$ will be positive because this term describes how fluctuations are transferred on average to the sub-grid gradients from the filtered gradients, analogous to the kinetic and scalar variance cascades which are downscale in three dimensions.

Using the same scaling approach discussed in § 2 but now for the filtered variables leads to

$$\frac{|N \langle \tilde{\mathbf{B}} \cdot \tilde{\mathbf{A}}^\top \cdot \mathbf{e}_z \rangle|}{|\langle \tilde{\mathbf{B}} \cdot \tilde{\mathbf{A}}^\top \cdot \tilde{\mathbf{B}} \rangle|} \sim O(\tilde{\Lambda}_B), \quad (2.25)$$

where $\tilde{\Lambda}_B \equiv N/\sqrt{\langle \|\tilde{\mathbf{B}}\|^2 \rangle}$. Therefore, at scales where $\tilde{\Lambda}_B \ll 1$, the balance reduces to

$$-\langle \tilde{\mathbf{B}} \cdot \tilde{\mathbf{A}}^\top \cdot \tilde{\mathbf{B}} \rangle \sim \langle \tilde{\mathbf{B}} \cdot \nabla \nabla \cdot \boldsymbol{\tau}_\phi \rangle, \quad (2.26)$$

while at scales where $\tilde{\Lambda}_B \gg 1$ the balance reduces to

$$N \langle \tilde{\mathbf{B}} \cdot \tilde{\mathbf{A}}^\top \cdot \mathbf{e}_z \rangle \sim \langle \tilde{\mathbf{B}} \cdot \nabla \nabla \cdot \boldsymbol{\tau}_\phi \rangle. \quad (2.27)$$

Since $\langle \tilde{\mathbf{B}} \cdot \nabla \nabla \cdot \boldsymbol{\tau}_\phi \rangle > 0$, then we must have $N \langle \tilde{\mathbf{B}} \cdot \tilde{\mathbf{A}}^\top \cdot \mathbf{e}_z \rangle > 0$ at scales where $\tilde{\Lambda}_B \gg 1$ in order for the balance to be satisfied. Therefore, although $\lim_{\ell/\eta_B \rightarrow 0} N \langle \tilde{\mathbf{B}} \cdot \tilde{\mathbf{A}}^\top \cdot \mathbf{e}_z \rangle \rightarrow \langle \mathcal{P}_{B2} \rangle$ is predicted to be negative due to the ramp-cliff structures, at scales where $\tilde{\Lambda}_B \gg 1$ is satisfied then $N \langle \tilde{\mathbf{B}} \cdot \tilde{\mathbf{A}}^\top \cdot \mathbf{e}_z \rangle > 0$. Hence, the role of this mean gradient term in the equation governing $\langle \|\tilde{\mathbf{B}}\|^2 \rangle$ changes with scale, providing a source for $\langle \|\tilde{\mathbf{B}}\|^2 \rangle$ at scales where $\tilde{\Lambda}_B \gg 1$, and providing a sink for $\langle \|\tilde{\mathbf{B}}\|^2 \rangle$ at scales where $\tilde{\Lambda}_B \ll 1$.

Note that regardless of Re_λ or Pr , there will always be a range of scales where $\tilde{\Lambda}_B \gg 1$ is satisfied because statistical homogeneity of the flow enforces that $\lim_{\ell/L_\phi \rightarrow \infty} \tilde{\mathbf{B}} \rightarrow 0$ (where L_ϕ is the integral length scale of ϕ), i.e. for sufficiently large scales, $\tilde{\mathbf{B}}$ is equivalent to the spatial average of \mathbf{B} , which is zero. Due to this, $\lim_{\ell/L_\phi \rightarrow \infty} \tilde{\Lambda}_B \rightarrow \infty$, regardless of Re_λ or Pr .

3. Theory: gradient dynamics in stably stratified turbulence

Having considered the case of passive scalars we now turn to consider stably stratified turbulence. We will see that some of the effects that are already present for passive scalars play an important role in understanding stratified turbulence, and in particular, the role of $\langle \mathcal{P}_{B2} \rangle$. As discussed earlier, the term $\langle \mathcal{P}_{B2} \rangle$ is expected to be unimportant compared with $\langle \mathcal{P}_{B1} \rangle$ for passive scalars in turbulent flows for which the particular value of N (on which $\langle \mathcal{P}_{B2} \rangle$ explicitly depends) is essentially irrelevant due to the linearity of the scalar equation. This is not true for stratified turbulent flows, however, because the momentum equation depends on N through the buoyancy term, and the momentum equation is nonlinear. Therefore, we anticipate that $\langle \mathcal{P}_{B2} \rangle$ could play an important role in stratified turbulence, and this suggests that the striking effect of Pr on $\langle \epsilon \rangle$ and $\langle \chi \rangle$ observed in Riley *et al.* (2023), which is much stronger than the Pr effect on $\langle \chi \rangle$ for passive scalars, could be connected to a Pr -dependence of $\langle \mathcal{P}_{B2} \rangle$.

3.1. Buoyancy acts as both a source and a sink for velocity gradients in stratified turbulence

The only difference between the gradient dynamics of passive scalar turbulence and stratified turbulence is the buoyancy term in the equation for \mathbf{S} . For a statistically

homogeneous flow, the equation governing $\langle \|\mathbf{S}\|^2 \rangle$ reduces to

$$\frac{1}{2} \partial_t \langle \|\mathbf{S}\|^2 \rangle = \langle \mathcal{P}_{S1} \rangle - \frac{N}{2} \langle \mathbf{S} : (\mathbf{B}e_z + e_z\mathbf{B}) \rangle - \langle \mathcal{D}_S \rangle + \langle \mathcal{P}_{S2} \rangle, \quad (3.1)$$

from which the pressure gradient term has disappeared because $\langle \mathbf{S} : \nabla \nabla p \rangle = 0$ for an incompressible, homogeneous flow. In this equation

$$\mathcal{P}_{S1} \equiv -\mathbf{S} : \mathbf{S} \cdot \mathbf{S} - (1/4)\mathbf{S} : \boldsymbol{\omega}\boldsymbol{\omega}, \quad (3.2)$$

where $-\mathbf{S} : \mathbf{S} \cdot \mathbf{S}$ is the strain self-amplification invariant, and $\mathbf{S} : \boldsymbol{\omega}\boldsymbol{\omega}$ is the enstrophy production invariant associated with the process of vortex stretching (Tsinober 2001). In a turbulent flow, $\langle \mathcal{P}_{S1} \rangle > 0$, reflecting the fact that nonlinearity in the flow self-amplifies the straining motion. We also note that using the results from Betchov (1956) for an incompressible, homogeneous flow, it can be shown that $\langle \mathcal{P}_{S1} \rangle = (1/2)\langle \mathcal{P}_{A1} \rangle$, where \mathcal{P}_{A1} is defined in (2.18). The dissipation term is $\mathcal{D}_S \equiv \nu \|\nabla \mathbf{S}\|^2$, and $\mathcal{P}_{S2} \equiv \mathbf{S} : \nabla \mathbf{F}_S$, which describes the contribution to the strain from the forcing (which is usually negligible in the equation for a high Reynolds number flow).

The buoyancy term that appears in (3.1) is $-(N/2)\langle \mathbf{S} : (\mathbf{B}e_z + e_z\mathbf{B}) \rangle$. However, it is straightforward to show that for an incompressible, homogeneous flow $\langle \mathbf{S} : (\mathbf{B}e_z + e_z\mathbf{B}) \rangle = \langle \mathbf{B} \cdot \mathbf{A}^\top \cdot e_z \rangle$, and therefore the buoyancy term in (3.1) is equal to $-(1/2)\langle \mathcal{P}_{B2} \rangle$. It was argued in § 2.2 that for a passive scalar with $\mathbf{B}(0) = \mathbf{0}$, for $t \ll \tau_\eta$ we have $\langle \mathcal{P}_{B2} \rangle > 0$, however, once the ramp-cliff structures form and the stationary regime $\partial_t \langle \|\mathbf{B}\|^2 \rangle = 0$ is attained, $\langle \mathcal{P}_{B2} \rangle < 0$. The argument that $\langle \mathcal{P}_{B2} \rangle < 0$ at long times is statistical in nature, and depends only on the assumption that there are ramp-cliff structures in the flow which correspond to a higher probability of $e_B \cdot e_z > 0$ events than $e_B \cdot e_z < 0$ events. Since ramp-cliff structures also occur in stratified flows (Riley *et al.* 2023) then the arguments given in § 2.2 regarding the sign of $\langle \mathcal{P}_{B2} \rangle$ also apply to stratified flows. Therefore, since $-(N/2)\langle \mathbf{S} : (\mathbf{B}e_z + e_z\mathbf{B}) \rangle = -(1/2)\langle \mathcal{P}_{B2} \rangle$, then the buoyancy term in (3.1) will act as a sink term for $t \ll \tau_\eta$, but will act as a source term once $\langle \mathcal{P}_{B2} \rangle < 0$ is established, contributing to the growth of $\langle \|\mathbf{S}\|^2 \rangle$, and hence acting to increase $\langle \epsilon \rangle = 2\nu \langle \|\mathbf{S}\|^2 \rangle$. Moreover, since $2\langle \|\mathbf{S}\|^2 \rangle = \langle \|\boldsymbol{\omega}\|^2 \rangle$ for an incompressible, homogeneous flow (Betchov 1956), this also implies that buoyancy acts to increase enstrophy in the flow.

This conclusion seems surprising, because in stably stratified turbulence, buoyancy is expected to play the role of a sink term for turbulence. To understand the role of buoyancy on the velocity gradients in more detail we can use the filtering approach introduced earlier. Applying the filtering operator to (2.1) and taking the gradient of the resulting equation yields

$$\tilde{D}_t \tilde{\mathbf{A}} = -\tilde{\mathbf{A}} \cdot \tilde{\mathbf{A}} - \nabla \nabla \tilde{p} + \nu \nabla^2 \tilde{\mathbf{A}} - N \tilde{\mathbf{B}} e_z + \nabla \tilde{\mathbf{F}} - \nabla \nabla \cdot \boldsymbol{\tau}_u, \quad (3.3)$$

where $\boldsymbol{\tau}_u \equiv \tilde{\mathbf{u}}\tilde{\mathbf{u}} - \tilde{\mathbf{u}}\tilde{\mathbf{u}}$ is the sub-grid stress tensor. From (3.3), the equation governing $\partial_t \langle \|\tilde{\mathbf{A}}\|^2 \rangle$ can be constructed, and for a statistically stationary, homogeneous flow it reduces to

$$0 = -\langle \tilde{\mathbf{A}} : (\tilde{\mathbf{A}} \cdot \tilde{\mathbf{A}}) \rangle - \nu \langle \|\nabla \tilde{\mathbf{A}}\|^2 \rangle - N \langle \tilde{\mathbf{B}} \cdot \tilde{\mathbf{A}}^\top \cdot e_z \rangle + \langle \tilde{\mathbf{A}} : \nabla \tilde{\mathbf{F}} \rangle - \langle \tilde{\mathbf{A}} : \nabla \nabla \cdot \boldsymbol{\tau}_u \rangle. \quad (3.4)$$

Once again, the pressure gradient term does not appear because $\langle \tilde{\mathbf{A}} : \nabla \nabla \tilde{p} \rangle = 0$ for an incompressible, homogeneous flow. The term $\langle \tilde{\mathbf{A}} : \nabla \nabla \cdot \boldsymbol{\tau}_u \rangle$ will be positive because this term describes how fluctuations are transferred on average to the sub-grid gradients from the filtered gradients, analogous to the kinetic energy cascade which is downscale in three dimensional stratified turbulence (Lindborg 2006).

For $\ell \gg \eta$ the dissipation term $\nu \langle \|\nabla \tilde{\mathbf{A}}\|^2 \rangle$ can be ignored because almost all of the dissipation takes place at scales $\ell = O(\eta)$, leading to the reduced balance

$$\langle \tilde{\mathbf{A}} : \nabla \tilde{\mathbf{F}} \rangle \sim \langle \tilde{\mathbf{A}} : (\tilde{\mathbf{A}} \cdot \tilde{\mathbf{A}}) \rangle + N \langle \tilde{\mathbf{B}} \cdot \tilde{\mathbf{A}}^\top \cdot \mathbf{e}_z \rangle + \langle \tilde{\mathbf{A}} : \nabla \nabla \cdot \boldsymbol{\tau}_u \rangle. \quad (3.5)$$

Using the same scaling approach discussed in § 2 but now for the filtered variables leads to

$$\frac{|N \langle \tilde{\mathbf{B}} \cdot \tilde{\mathbf{A}}^\top \cdot \mathbf{e}_z \rangle|}{|\langle \tilde{\mathbf{A}} : (\tilde{\mathbf{A}} \cdot \tilde{\mathbf{A}}) \rangle|} \sim O(\tilde{\Lambda}_A), \quad (3.6)$$

$$\tilde{\Lambda}_A \equiv \frac{N \langle \|\tilde{\mathbf{B}}\|^2 \rangle^{1/2}}{\langle \|\tilde{\mathbf{A}}\|^2 \rangle}. \quad (3.7)$$

In the regime $\tilde{\Lambda}_A \gg 1$ the balance in (3.5) reduces to

$$\langle \tilde{\mathbf{A}} : \nabla \tilde{\mathbf{F}} \rangle \sim N \langle \tilde{\mathbf{B}} \cdot \tilde{\mathbf{A}}^\top \cdot \mathbf{e}_z \rangle + \langle \tilde{\mathbf{A}} : \nabla \nabla \cdot \boldsymbol{\tau}_u \rangle, \quad (3.8)$$

and if we also have $\tilde{\Lambda}_B \gg 1$ then as shown in § 2.3, $N \langle \tilde{\mathbf{B}} \cdot \tilde{\mathbf{A}}^\top \cdot \mathbf{e}_z \rangle > 0$. This represents the balance at relatively large scales where the production term due to forcing is balanced by losses due to buoyancy and transfer to smaller scales (which is analogous to the TKE equation (2.3) because the TKE is dominated by the large scales in high Reynolds number flows). The role of the buoyancy term $-N \langle \tilde{\mathbf{B}} \cdot \tilde{\mathbf{A}}^\top \cdot \mathbf{e}_z \rangle$ is therefore subtle, opposing the production of velocity gradients at scales where $\tilde{\Lambda}_B \gg 1$, but aiding their production at scales where $\tilde{\Lambda}_B \ll 1$. This must be connected to the observation in Legaspi & Waite (2020) based on their numerical simulations that the buoyancy spectrum changes sign and indicates transfer of potential energy to kinetic energy at high wavenumbers in stratified turbulence. An investigation into this connection will be the subject of future work.

Note that in a flow where $\tilde{\Lambda}_B \geq O(1) \forall \ell$, the buoyancy term will act as a sink term for the velocity gradients at all scales and corresponds to the case where buoyancy is strong enough to suppress turbulence at all scales.

3.2. Prandtl number dependence of the kinetic and potential energy dissipation rates

Having considered how stratification impacts the velocity gradients through the buoyancy term, we now want to understand the impact of varying Pr in order to understand how Pr affects $\langle \epsilon \rangle$ and $\langle \chi \rangle$ in stratified turbulence. Although a general analytical treatment of this problem is not possible, we can obtain some insights by considering a limiting case.

In § 2 the following scaling estimate was obtained:

$$\frac{\|-(N/2)(\mathbf{B}\mathbf{e}_z + \mathbf{e}_z\mathbf{B})\|}{\|-\mathbf{S} \cdot \mathbf{S} - (1/4)(\boldsymbol{\omega}\boldsymbol{\omega} - \|\boldsymbol{\omega}\|^2\mathbf{I}) - \nabla\nabla p\|} \sim O(\Lambda_S), \quad (3.9)$$

and given that the equation is regular in the limit $\Lambda_S \rightarrow 0$, this suggests that we can use Λ_S as an expansion parameter and consider the regime $\Lambda_S \ll 1$ where the effects of stratification on the gradient fields are weak.

Using the scaled variables $\mathbf{A}^* \equiv \mathbf{A}/\sigma_A$ and $\mathbf{B}^* \equiv \mathbf{B}/\sigma_B$, we therefore introduce the expansions

$$\mathbf{A}^* = \sum_{p=0}^{\infty} \mathbf{A}_{(p)}^* \Lambda_S^p, \tag{3.10}$$

$$\mathbf{B}^* = \sum_{p=0}^{\infty} \mathbf{B}_{(p)}^* \Lambda_S^p, \tag{3.11}$$

where $\mathbf{A}_{(0)}^*$ and $\mathbf{B}_{(0)}^*$ correspond to the solutions for the passive scalar limit $\Lambda_S \rightarrow 0$, and $\mathbf{A}_{(p)}^*$ and $\mathbf{B}_{(p)}^*$ for $p \geq 1$ can be obtained by inserting the expansions into the evolution equations for \mathbf{A}^* and \mathbf{B}^* . Using these expansions we obtain for $\Lambda_S \ll 1$

$$\begin{aligned} |\langle \mathcal{P}_{B2} \rangle| &= N |\langle \mathbf{B}_{(0)} \cdot \mathbf{A}_{(0)}^\top \cdot \mathbf{e}_z \rangle + \Lambda_S \langle \mathbf{B}_{(0)} \cdot \mathbf{A}_{(1)}^\top \cdot \mathbf{e}_z \rangle + \Lambda_S \langle \mathbf{B}_{(1)} \cdot \mathbf{A}_{(0)}^\top \cdot \mathbf{e}_z \rangle| + O(\Lambda_S^2) \\ &\sim O(N\sigma_{A0}\sigma_{B0}[1 + 2\Lambda_S]), \end{aligned} \tag{3.12}$$

where higher-order terms have been dropped, and where $\sigma_{A0} \equiv \sqrt{\langle \|\mathbf{A}_{(0)}\|^2 \rangle}$ and $\sigma_{B0} \equiv \sqrt{\langle \|\mathbf{B}_{(0)}\|^2 \rangle}$.

Since $\mathbf{A}_{(0)}$ corresponds to the solution in the passive scalar limit, σ_{A0} is independent of Pr . If $\langle \chi \rangle$ exhibits anomalous behaviour with respect to Pr for a passive scalar then $\sigma_{B0} \propto Pr^{1/2}$. The results of Donzis *et al.* (2005), which were discussed in § 2.1, imply that unless Re_λ is sufficiently large then although σ_{B0} grows with Pr , the growth is not anomalous. Indeed, their results imply that for finite Re_λ , $\sigma_{B0} \propto Pr^{1/2} / \ln(Pr)$ in the limit $Pr \rightarrow \infty$. Crucially for our purposes, however, the fact that σ_{B0} is an increasing function of Pr for $Pr > 1$ implies through (3.12) that for a given Reynolds number, $|\langle \mathcal{P}_{B2} \rangle|$ will grow with increasing Pr in the regime $\Lambda_S \ll 1$.

The limitation of this argument, however, is that the scaling estimate on the second line of (3.12) ignores the effect of alignments between the tensors, e.g. between $\mathbf{B}_{(0)} \cdot \mathbf{A}_{(0)}^\top$ and \mathbf{e}_z , and the fact that these alignments may also depend on Pr . While the argument of the preceding paragraph would suggest that $|\langle \mathcal{P}_{B2} \rangle|$ will grow indefinitely with increasing Pr , symmetry considerations based on the tensor alignments suggest that the growth must saturate at sufficiently large Pr . These considerations are motivated by a number of studies that show that for the case of a passive scalar driven by a mean-scalar gradient in isotropic turbulence, although anisotropy of \mathbf{B} persists for arbitrarily large Re_λ for $Pr = O(1)$, the anisotropy weakens when Pr is increased beyond $O(1)$ (Sreenivasan 2018; Buaria *et al.* 2021a; Shete *et al.* 2022). For example, Shete *et al.* (2022) developed a model which suggests that the skewness of B_z scales as $\sim O(Pr^{-1/2} Re_\lambda^0)$, which is supported by their DNS results. Since the scalar gradients are dominated by the smallest scales in the scalar field, this suggests that in the regime $Pr \gg 1$ there will be a scale $\ell_{iso} \ll \eta$ below which the scalar gradients are approximately isotropic. In view of this, we introduce the decompositions $\mathbf{B} = \tilde{\mathbf{B}} + \mathbf{B}'$ and $\mathbf{A} = \tilde{\mathbf{A}} + \mathbf{A}'$, where the prime denotes the sub-grid field variable, and then write the zeroth-order contribution to $\langle \mathcal{P}_{B2} \rangle$ as

$$\begin{aligned} N \langle \mathbf{B}_{(0)} \cdot \mathbf{A}_{(0)}^\top \cdot \mathbf{e}_z \rangle &= N \langle \tilde{\mathbf{B}}_{(0)} \cdot \tilde{\mathbf{A}}_{(0)}^\top \rangle \cdot \mathbf{e}_z + N \langle \tilde{\mathbf{B}}_{(0)} \cdot (\mathbf{A}'_{(0)})^\top \rangle \cdot \mathbf{e}_z \\ &\quad + N \langle \mathbf{B}'_{(0)} \cdot \tilde{\mathbf{A}}_{(0)}^\top \rangle \cdot \mathbf{e}_z + N \langle \mathbf{B}'_{(0)} \cdot (\mathbf{A}'_{(0)})^\top \rangle \cdot \mathbf{e}_z. \end{aligned} \tag{3.13}$$

If the filter length ℓ satisfies $\ell \gg \eta_B$, then ignoring the effects of intermittency, $\tilde{\mathbf{B}}_{(0)}$ will be independent of Pr (and by definition, $\tilde{\mathbf{A}}_{(0)}$ and $\mathbf{A}'_{(0)}$ are also independent of Pr). However,

$\|\mathbf{B}'_{(0)}\|$ will grow with increasing Pr , and a simple scaling estimate of the sizes of $N\langle\mathbf{B}'_{(0)} \cdot \tilde{\mathbf{A}}_{(0)}^\top\rangle \cdot \mathbf{e}_z$ and $N\langle\mathbf{B}'_{(0)} \cdot (\mathbf{A}'_{(0)})^\top\rangle \cdot \mathbf{e}_z$ would then suggest that these terms (and hence also $N\langle\mathbf{B}_{(0)} \cdot \mathbf{A}_{(0)}^\top\rangle \cdot \mathbf{e}_z$) will grow in magnitude with increasing Pr . This is effectively what the scaling estimate in (3.12) captures. What this argument misses, however, is that the growth of $N\langle\mathbf{B}'_{(0)} \cdot \tilde{\mathbf{A}}_{(0)}^\top\rangle \cdot \mathbf{e}_z$ and $N\langle\mathbf{B}'_{(0)} \cdot (\mathbf{A}'_{(0)})^\top\rangle \cdot \mathbf{e}_z$ with increasing Pr can only occur if $\mathbf{B}'_{(0)}$ is an anisotropic field. If it were isotropic then symmetry considerations enforce $\langle\mathbf{B}'_{(0)} \cdot \tilde{\mathbf{A}}_{(0)}^\top\rangle = \mathbf{0}$ and $\langle\mathbf{B}'_{(0)} \cdot (\mathbf{A}'_{(0)})^\top\rangle = \mathbf{0}$ because $\mathbf{B}'_{(0)} \cdot \tilde{\mathbf{A}}_{(0)}^\top$ and $\mathbf{B}'_{(0)} \cdot (\mathbf{A}'_{(0)})^\top$ are first-order tensors whose mean must be zero if they are isotropically distributed. If $\ell \gg \eta_B \geq O(\ell_{iso})$ then $\mathbf{B}'_{(0)}$ will be anisotropic and the simple scaling estimates that suggest that $N\langle\mathbf{B}'_{(0)} \cdot \tilde{\mathbf{A}}_{(0)}^\top\rangle \cdot \mathbf{e}_z$ and $N\langle\mathbf{B}'_{(0)} \cdot (\mathbf{A}'_{(0)})^\top\rangle \cdot \mathbf{e}_z$ grow with Pr are reasonable. However, if Pr is large enough for there to exist a range of scales $\eta_B \ll \ell \leq \ell_{iso}$, then for ℓ in this range $\mathbf{B}'_{(0)}$ will be an approximately isotropic field and equation (3.13) would reduce to

$$N\langle\mathbf{B}_{(0)} \cdot \mathbf{A}_{(0)}^\top\rangle \cdot \mathbf{e}_z \approx N\langle\tilde{\mathbf{B}}_{(0)} \cdot \tilde{\mathbf{A}}_{(0)}^\top\rangle \cdot \mathbf{e}_z + N\langle\tilde{\mathbf{B}}_{(0)} \cdot (\mathbf{A}'_{(0)})^\top\rangle \cdot \mathbf{e}_z, \tag{3.14}$$

which is approximately independent of Pr . Hence, once Pr is large enough for there to exist a range of scales $\eta_B \ll \ell \leq \ell_{iso}$, then $N\langle\mathbf{B}_{(0)} \cdot \mathbf{A}_{(0)}^\top\rangle \cdot \mathbf{e}_z$ will saturate to the approximately Pr -independent value given by the right-hand side of (3.14). The same argument can also be made regarding the sub-leading terms in (3.12).

These considerations suggest the following: the scaling estimate in (3.12) that predicts $|\langle\mathcal{P}_{B2}\rangle|$ grows with Pr should be reasonable, except that the growth rate with Pr will be slower than predicted by (3.12) due to the fact that the Pr -dependence of the anisotropy of $\mathbf{B}_{(0)} \cdot \mathbf{A}_{(0)}^\top$ is not accounted for in the scaling estimate. However, once Pr becomes large enough for the condition $\eta_B \ll \ell_{iso}$ to be satisfied, then the growth of $|\langle\mathcal{P}_{B2}\rangle|$ with Pr will saturate, and we denote this saturation Prandtl number by Pr_S . Recalling that $\ell_{iso} \ll \eta$, then the minimum Pr required to obtain $\eta_B \ll \ell_{iso}$ could be estimated as the value of Pr at which $\eta/\eta_B = O(10)$. Since $\eta_B = \eta Pr^{-1/2}$ this yields $Pr = O(100)$, implying that at minimum $Pr_S = O(100)$.

Having considered the dependence of $\langle\mathcal{P}_{B2}\rangle$ on Pr , we can now consider how this will impact $\langle\epsilon\rangle$ and $\langle\chi\rangle$. Since $\langle\mathcal{P}_{B2}\rangle < 0$, then in the regime $\Lambda_S \ll 1$, as Pr increases the buoyancy term $-(N/2)\langle\mathbf{S} : (\mathbf{B}\mathbf{e}_z + \mathbf{e}_z\mathbf{B})\rangle = -(1/2)\langle\mathcal{P}_{B2}\rangle$ in the equation for $\langle\|\mathbf{S}\|^2\rangle$ grows and hence $\langle\epsilon\rangle$ will also grow with Pr . On the other hand, this term appears with the opposite sign in the equation for $\langle\|\mathbf{B}\|^2\rangle$ as $\langle\mathcal{P}_{B2}\rangle$, and therefore as Pr increases, this term increasingly opposes the production of $\langle\|\mathbf{B}\|^2\rangle$ which would then act to cause $\langle\chi\rangle$ to decrease as Pr increases. This behaviour predicted by the asymptotic analysis agrees qualitatively with the DNS results in Riley *et al.* (2023), where it was shown that $\langle\epsilon\rangle$ increases and $\langle\chi\rangle$ decreases as Pr is increased from 1 to 7. Since $\langle\mathcal{P}_{B2}\rangle$ appears with a pre-factor of 1/2 in the equation for $\langle\|\mathbf{S}\|^2\rangle$ but with a pre-factor of unity in the equation for $\langle\|\mathbf{B}\|^2\rangle$, then we would anticipate that the effect of Pr via $\langle\mathcal{P}_{B2}\rangle$ will be stronger on $\langle\chi\rangle$ than on $\langle\epsilon\rangle$, which is again consistent with the DNS results in Riley *et al.* (2023). This enhancement of $\langle\epsilon\rangle$ and suppression of $\langle\chi\rangle$ due to $\langle\mathcal{P}_{B2}\rangle$ as Pr increases is predicted to persist up to $Pr = O(Pr_S)$. Finally, we note that the importance of this effect on $\langle\epsilon\rangle$ is determined by the size of Λ_S , and vanishes for the passive scalar limit $\Lambda_S \rightarrow 0$ for which $\langle\mathcal{P}_{B2}\rangle/\langle\mathcal{P}_{S1}\rangle \rightarrow 0$. Its effect on $\langle\chi\rangle$ is determined by the size of Λ_B , and vanishes in the limit $\Lambda_B \rightarrow 0$ for which $\langle\mathcal{P}_{B2}\rangle/\langle\mathcal{P}_{B1}\rangle \rightarrow 0$.

In the regime $\Lambda_S \geq O(1)$, it is not possible to explore analytically the effect of Pr on the velocity and density gradient dynamics without either renormalizing the expansion in Λ_S (i.e. using some method to partially sum the divergent series) or else introducing

closure approximations. We can observe, however, that when $\Lambda_S \geq O(1)$, provided $\langle \mathcal{P}_{B2} \rangle$ remains negative, then σ_A and σ_B will still grow with increasing Pr since the equation governing $\|\mathbf{B}\|^2$ guarantees that the magnitude of σ_B will increase with increasing Pr provided only that $\langle \mathcal{P}_{B1} \rangle + \langle \mathcal{P}_{B2} \rangle > 0$ (which must be satisfied for a statistically stationary system). Therefore, the scaling estimate $|\langle \mathcal{P}_{B2} \rangle| \sim O(N\sigma_A\sigma_B)$ suggests that $|\langle \mathcal{P}_{B2} \rangle|$ will grow with increasing Pr even for $\Lambda_S \geq O(1)$, and so $\langle \epsilon \rangle$ will increase with increasing Pr while $\langle \chi \rangle$ will decrease. While we argued that this effect of Pr saturates at $Pr = O(Pr_S)$ for the weakly stratified regime $\Lambda_S \ll 1$, it is not obvious that this should be so for the regime $\Lambda_S \geq O(1)$. The reason for this is twofold. First, \mathbf{A} will not be isotropic when $\Lambda_S \geq O(1)$, and second, results in Riley *et al.* (2023) show that the skewness of \mathbf{B} increases in stratified turbulence as Pr is increased. Hence the arguments given earlier for why the growth of $\langle \mathcal{P}_{B2} \rangle$ must saturate at $Pr = O(Pr_S)$ for the regime $\Lambda_S \ll 1$ do not seem to apply for the regime $\Lambda_S \geq O(1)$.

3.3. The appropriate estimate for the importance of buoyancy on the gradient fields

The analysis just presented suggests that the relative sizes of the buoyancy and inertial forces in the equation for $\langle \|\mathbf{S}\|^2 \rangle$ will depend upon Pr . This has significant implications for whether the standard buoyancy Reynolds number can be used to reliably estimate the impact of buoyancy on the smallest scales of the flow, and the question of in which parameter regimes the behaviour of the velocity and density gradients in stratified turbulence approach those of passive scalars.

Riley & de Bruyn Kops (2003) proposed a buoyancy Reynolds number $Re_b \equiv ReFr^2$, where the Reynolds number Re and Froude number Fr are based on the horizontal integral length scale L_h and the r.m.s. horizontal velocity U_h of the flow. The parameter Re_b was based on a scaling analysis developed in Riley & de Bruyn Kops (2003) to estimate when the local gradient Richardson number will be less than one, and their analysis showed that this will be satisfied when $Re_b > 1$. When $Re_b > O(1)$ it is usually assumed that the effect of buoyancy on the smallest flow scales will be sub-leading, and negligible when $Re_b \gg 1$ (Riley & Lindborg 2012). The activity parameter $Gn \equiv \langle \epsilon \rangle / (\nu N^2)$ (Gibson 1980; Gargett, Osborn & Nasmyth 1984) is also often used instead of Re_b , and $Re_b \sim O(Gn)$ provided that Gn is large enough for Taylor scaling for the dissipation $\langle \epsilon \rangle \sim O(U_h^3/L_h)$ to hold (de Bruyn Kops & Riley 2019; Bragg & de Bruyn Kops 2024).

In § 2 we showed that in the equation for \mathbf{S} , the ratio of the buoyancy to inertial terms is of order $\Lambda_S \equiv N\sigma_B/\sigma_S^2$. This parameter can be re-expressed in terms of more familiar parameters as

$$\Lambda_S = 2Pr^{1/2}Gn^{-1/2}\Gamma^{1/2}, \tag{3.15}$$

where $\Gamma \equiv \langle \chi \rangle / \langle \epsilon \rangle$ is the mixing coefficient. For $Pr = 1$, it is known that when $Gn \gg 1$ and $Fr \ll 1$ (the strongly stratified regime), $\Gamma \sim O(1)$ to leading order (Maffioli, Brethouwer & Lindborg 2016; Bragg & de Bruyn Kops 2024). In this case, $\Lambda_S \sim O(Gn^{-1/2})$, so that the sizes of Λ_S and Gn are directly related. However, even for this case, the condition for the effects of buoyancy on the velocity gradients to be small is not simply $Gn \gg 1$ but the more restrictive condition $Gn^{1/2} \gg 1$. Furthermore, when $Pr = 1$, $Gn \gg 1$ and $Fr \gg 1$ (the weakly stratified regime), $\Gamma \sim O(Fr^{-2})$ (Maffioli *et al.* 2016; Bragg & de Bruyn Kops 2024) so that $\Lambda_S \sim O(Gn^{-1/2}Fr^{-1}) \ll 1$. For $Pr \neq O(1)$, there is no simple relationship between Λ_S and Gn , and therefore the size of Gn may not provide a reliable estimate for the importance of buoyancy on the small scales, which should instead be estimated using Λ_S .

Whether this matters in practice as a way of gauging the impact of buoyancy on the smallest flow scales depends upon the relevant ranges of Gn and Pr . For example, if $Gn \gg 1$, then unless Pr is very large, we will have $\Lambda_S \ll 1$. In this case having $Gn \gg 1$ would lead to the correct conclusion that the effects of buoyancy on the velocity gradients are negligible. For temperature stratified air and water $Pr \leq O(10)$, and over this range then provided $Gn \gg 1$, Λ_S will likely be small enough for the effects of buoyancy on \mathbf{S} and \mathbf{B} to be small. However, for salt-stratified water $Pr = O(1000)$, and this may cause Λ_S to be large enough for the effects of buoyancy on \mathbf{S} and \mathbf{B} to be important even when $Gn \gg 1$. Moreover, field observations in oceanic stratified flows show that Gn has a large range of values, spanning $O(10^{-2}) \leq Gn \leq O(10^5)$ (see figure 14 of Jackson & Rehmann 2014). This, together with the relevant ranges of Pr , indicates that in oceanic contexts, Λ_S should be used to determine the importance of buoyancy on the smallest flow scales rather than Gn , since the latter does not correctly capture the impact of Pr on the importance of buoyancy on the velocity gradient dynamics.

4. Direct numerical simulations

Data sets from DNSs will be used to explore the predictions and insights from the theoretical analysis. The first is a DNS of passive scalars which was previously reported in Shete & de Bruyn Kops (2020) and Shete *et al.* (2022). Specifically, we look at the DNS denoted in those papers as R633, with Taylor Reynolds number of 633, and where $Pr = 0.1, 1, 7$ are resolved using 8190^3 , 8190^3 and 14256^3 grid points, respectively. The velocity field is homogeneous and isotropic, and is forced to be very nearly statistically stationary as described later in this section. There is a constant mean scalar gradient in the z -direction so that the scalar field is homogeneous in all directions, and the statistics are independent of direction in the horizontal.

The second data set is of stably stratified turbulence which was previously reported in de Bruyn Kops & Riley (2019) and Riley *et al.* (2023). The velocity field is forced to achieve homogeneous and isotropic turbulence, and then allowed to decay until it exhibits power-law decay with Taylor Reynolds number of 335, at which time the density field is initialized with zero fluctuations and allowed to decay subject to buoyancy. Simulations with $Pr = 1$ and $Pr = 7$ are considered which are resolved using grids of size $8192^2 \times 4096$ and $12288^2 \times 6144$, respectively, and in each case the domain is twice as large in the horizontal than the vertical directions. For both cases, $Fr \approx 0.3$ when the density field is initialized and decreases by a factor of approximately 10 within eight buoyancy periods. The value of Gn changes from approximately 65 to approximately 20 in the same time. See figure 1 in Riley *et al.* (2023) for more details, noting the difference in the definition of the Froude number (their definition includes a factor of 2π).

For all the simulations, the domain is triply periodic so that a Fourier spectral method can be used to evolve the flows in time with minimal phase or truncation errors. Derivatives and addition are done in Fourier space, multiplication is done in real space, a third-order Runge–Kutta schema is used to advance the solutions in time, and dealiasing is done with a combination of phase shifting, spectral truncation and alternating between the advective and conservative forms of the nonlinear terms. In decaying simulations, care must be taken with large-scale resolution (de Bruyn Kops & Riley 1998), and small-scale resolution is important in all DNS; the resolution characteristics of the simulations used here are reported in detail in Shete & de Bruyn Kops (2020) and Riley *et al.* (2023).

The simulations require the specification of a forcing term \mathbf{F} in the momentum equation either to maintain the velocity field in a quasi-stationary state (for the passive scalar cases)

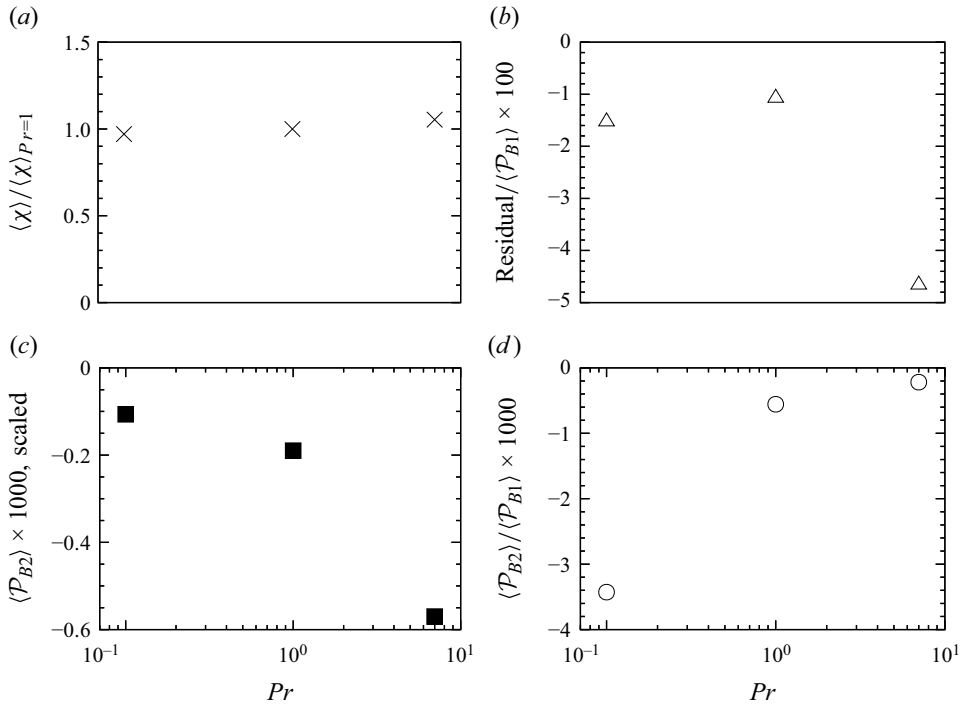


Figure 1. Results for (a) $\langle \chi \rangle$ normalized by its value for $Pr = 1$, (b) ‘residual’ which is the sum of the right-hand side of (2.14) normalized using $\langle \mathcal{P}_{B1} \rangle$ and multiplied by 100, (c) $\langle \mathcal{P}_{B2} \rangle / (\sigma_A N^2)$ multiplied by 1000, (d) ratio of production terms $\langle \mathcal{P}_{B2} \rangle / \langle \mathcal{P}_{B1} \rangle$ multiplied by 1000. Note that the same quantity plotted in (b) is termed ‘unsteadiness’ for the decaying simulations (see figure 3).

or to initialize the velocity field (for the stably stratified cases). The value of F is specified using a spring–damper model developed by Overholt & Pope (1998) and generalized for the stratified case in Rao & de Bruyn Kops (2011). The technique efficiently converges the velocity field to a prescribed spectrum at low wavenumbers.

5. Results and discussion

5.1. Passive scalars

We begin by considering results for passive scalars. In figure 1(a), the results for $\langle \chi \rangle$ as a function of Pr are considered, normalized by the reference value at $Pr = 1$, denoted by $\langle \chi \rangle_{Pr=1}$ (note that the vertical axis range used in the plot is chosen for fair comparison with the stratified results in figure 3 for which this range is necessary). Over the range $Pr \in [0.1, 7]$, $\langle \chi \rangle / \langle \chi \rangle_{Pr=1}$ increases with increasing Pr , with values going from approximately 0.97 to 1.05. To ensure that these variations are not due to a lack of stationarity of the scalar gradient field, in figure 1(b) we plot the ‘residual’, which is the sum of the right-hand side of (2.14), normalized by $\langle \mathcal{P}_{B1} \rangle$ (defined in (2.12)). The residual values are two orders of magnitude smaller than the dominant production term $\langle \mathcal{P}_{B1} \rangle$, which indicates that the observed variations of $\langle \chi \rangle / \langle \chi \rangle_{Pr=1}$ are not due to a lack of small-scale stationarity.

The variations observed for $\langle \chi \rangle / \langle \chi \rangle_{Pr=1}$ in the passive scalar case would probably be considered negligible from a practical standpoint given that this variation corresponds to varying Pr by two orders of magnitude. However, the variation could be considered

non-negligible from a theoretical standpoint as it might indicate that $\langle \chi \rangle$ does not approach a constant as Pr increases. In § 2.1 the model of Donzis *et al.* (2005) was discussed which in fact predicts that unless Re_λ is sufficiently high, $L\langle \chi \rangle / (U\langle \phi^2 \rangle)$ will vary with Pr at a rate that is proportional to $1 / \ln Pr$ for fixed Re_λ and $Pr \gg 1$. Direct numerical simulation results in Donzis *et al.* (2005) confirmed this model prediction, as does the more recent study of Buaria *et al.* (2021b) that considers the larger value of $Re_\lambda = 140$ with results spanning $Pr \in [1, 512]$. Our results do not reveal such a strong Pr dependence as theirs, but this is likely due to our DNS having the much higher value $Re_\lambda = 633$, noting that the model of Donzis *et al.* (2005) predicts that $\langle \chi \rangle$ will become independent of Pr (for finite Pr) in the limit $Re_\lambda \rightarrow \infty$. For our DNS with $Re_\lambda = 633$, the model of (2.10) predicts that the normalized dissipation rate $L\langle \chi \rangle / (U\langle \phi^2 \rangle)$ will vary by $\approx 6\%$ in going from $Pr = 1$ to $Pr = 7$, and this is close to the magnitude of the variation that we observe. However, the model predicts that $L\langle \chi \rangle / (U\langle \phi^2 \rangle)$ should decrease as Pr increases; while our data show that $L\langle \chi \rangle / (U\langle \phi^2 \rangle)$ decreases in going from $Pr = 0.1$ to $Pr = 1$, and increases in going from $Pr = 1$ to $Pr = 7$. This discrepancy could be due to a lack of statistical stationarity of the large scales of the passive scalar field in our DNS for $Pr = 7$. Indeed, our DNS for $Re_\lambda = 633$ and $Pr = 7$ is extremely demanding computationally, and we are only able to construct the statistics by averaging over one large-eddy turnover time. This averaging window is much less than that used for the $Pr = 0.1, 1$ cases, and is also much less than that used in the DNS of Buaria *et al.* (2021b) at the much lower value of $Re_\lambda = 140$. Regardless of whether a lack of stationarity in the $Pr = 7$ DNS explains the discrepancy or something else, what is far more important for the present study is that the variation of $\langle \chi \rangle / \langle \chi \rangle_{Pr=1}$ that we observe over the range $Pr \in [0.1, 7]$ for passive scalars is very small compared with what is observed for stratified flows, as will be shown in § 5.2.

In figure 1(c) we consider the mean production term $\langle \mathcal{P}_{B2} \rangle$ (defined in (2.13)), normalized using $\sigma_A N^2$. In agreement with the analysis in § 2.2, $\langle \mathcal{P}_{B2} \rangle$ is negative, which we argued is due to the emergence of ramp-cliff structures in the scalar field. Moreover, the magnitude of $\langle \mathcal{P}_{B2} \rangle$ increases as Pr increases, as was predicted in § 3.2. The analysis also suggested that this growth would persist up to $Pr = O(Pr_S)$, and we estimated that at minimum, $Pr_S = O(100)$. The results in figure 1(c) are consistent with this in that there is no indication of a saturation in the growth by $Pr = O(10)$.

As anticipated earlier, figure 1(d) shows that the ratio $\langle \mathcal{P}_{B2} \rangle / \langle \mathcal{P}_{B1} \rangle$ is very small, with the magnitude of $\langle \mathcal{P}_{B2} \rangle$ of the order of 1000 times smaller than $\langle \mathcal{P}_{B1} \rangle$. Hence, the mechanism associated with $\langle \mathcal{P}_{B2} \rangle$ that can affect the Pr -dependence of $\langle \chi \rangle$ is negligible for these passive scalar cases. The results also show that $\langle \mathcal{P}_{B2} \rangle / \langle \mathcal{P}_{B1} \rangle$ becomes smaller in magnitude as Pr increases. This can be understood from the scaling discussed in § 2 which suggests that $|\langle \mathcal{P}_{B2} \rangle / \langle \mathcal{P}_{B1} \rangle| \sim O(\Lambda_B)$, where $\Lambda_B \equiv N / \sigma_B$. As demonstrated in § 2, Λ_B is independent of N for a passive scalar (because σ_B is proportional to N), and since σ_B increases with increasing Pr , then Λ_B decreases as Pr increases.

A significant difference between the two production terms \mathcal{P}_{B1} and \mathcal{P}_{B2} relates to their behaviour in rotation and strain dominated regions of the flow. In particular, using the strain-rate \mathbf{S} and rotation-rate \mathbf{R} decomposition $\mathbf{A} = \mathbf{S} + \mathbf{R}$, we have $\mathcal{P}_{B1} \equiv -\mathbf{B} \cdot \mathbf{A}^\top \cdot \mathbf{B} = -\mathbf{B} \cdot \mathbf{S} \cdot \mathbf{B}$ due to the antisymmetry of \mathbf{R} . Rotation therefore does not directly contribute to the fluctuating gradient production term \mathcal{P}_{B1} , but only indirectly contributes by influencing the alignments of \mathbf{B} with respect to the eigenframe of \mathbf{S} . If we therefore conditionally average \mathcal{P}_{B1} on the invariant $Q \equiv -\mathbf{A} : \mathbf{A} / 2$, then we expect that the contribution to the average behaviour

$$\langle \mathcal{P}_{B1} \rangle = \int_{\mathbb{R}} \varphi(Q) \langle \mathcal{P}_{B1} \rangle_Q dQ, \tag{5.1}$$

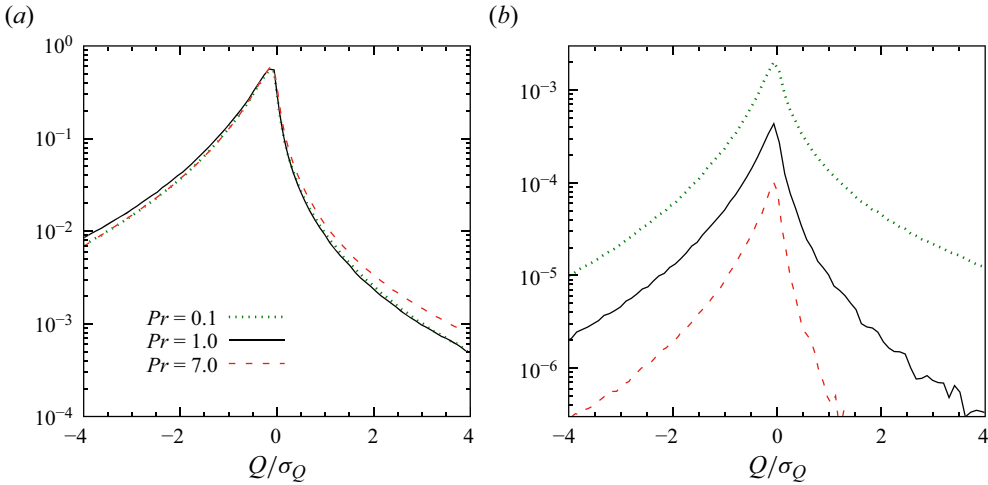


Figure 2. Results for (a) $\sigma_A \sigma_B^{-2} \varphi(Q) \langle \mathcal{P}_{B1} \rangle_Q$ and (b) $-\sigma_A \sigma_B^{-2} \varphi(Q) \langle \mathcal{P}_{B2} \rangle_Q$ for the passive scalar cases. The horizontal axis is normalized using $\sigma_Q \equiv \sqrt{\langle Q^2 \rangle}$.

(where $\varphi(Q)$ is the p.d.f. of Q) from rotation (or vorticity) dominated regions $Q > 0$ will be small compared with that from strain dominated regions $Q < 0$. On the other hand, the rotation contribution to $\langle \mathcal{P}_{B2} \rangle$, namely $N \langle \mathbf{B} \cdot (\mathbf{R} \cdot \mathbf{e}_z) \rangle$, is not zero because of the misalignment between \mathbf{B} and \mathbf{e}_z . As a result, the contribution to the average behaviour

$$\langle \mathcal{P}_{B2} \rangle = \int_{\mathbb{R}} \varphi(Q) \langle \mathcal{P}_{B2} \rangle_Q dQ, \tag{5.2}$$

from $Q > 0$ regions may be significant compared with that from $Q < 0$ regions. Taken together, this implies that the mean gradient production may play a much more significant role in governing $\|\mathbf{B}\|^2$ in rotation dominated regions than it does in strain dominated regions.

The results in figure 2 for $\sigma_A \sigma_B^{-2} \varphi(Q) \langle \mathcal{P}_{B1} \rangle_Q$ show that this quantity is significantly skewed towards strain dominated regions where $Q < 0$, and displays a weak dependence on Pr . This negative skewness comes entirely from $\langle \mathcal{P}_{B1} \rangle_Q$ because $\varphi(Q)$ is positively skewed in isotropic turbulence, which is associated with the vorticity field being more intermittent than the strain-rate field (Tsinober 2001). The implication is that the majority of the production associated with \mathcal{P}_{B1} occurs in strain dominated rather than rotation dominated regions of the flow, as expected. For $\sigma_A \sigma_B^{-2} \varphi(Q) \langle \mathcal{P}_{B2} \rangle_Q$ the behaviour is almost symmetric with respect to Q for $Pr = 0.1$, but becomes increasingly negatively skewed as Pr increases. The values of $\sigma_A \sigma_B^{-2} \varphi(Q) \langle \mathcal{P}_{B2} \rangle_Q$ decrease dramatically as Pr is increased (essentially because of the reduction of Λ_B with increasing Pr , discussed earlier), and at all Pr considered the values are so small that there are no regions of the flow where \mathcal{P}_{B2} plays a significant role in the production of the scalar gradients relative to \mathcal{P}_{B1} . From the scaling estimates, this can again be understood as a consequence of the flows considered being in the regime where the parameter $\Lambda_B \equiv N/\sigma_B$ is very small. We will return later to consider $\sigma_A \sigma_B^{-2} \varphi(Q) \langle \mathcal{P}_{B2} \rangle_Q$ in the context of stratified flows, where its dependence on Q can give insights into how the buoyancy term might behave differently in strain and rotation dominated regions of the flow.

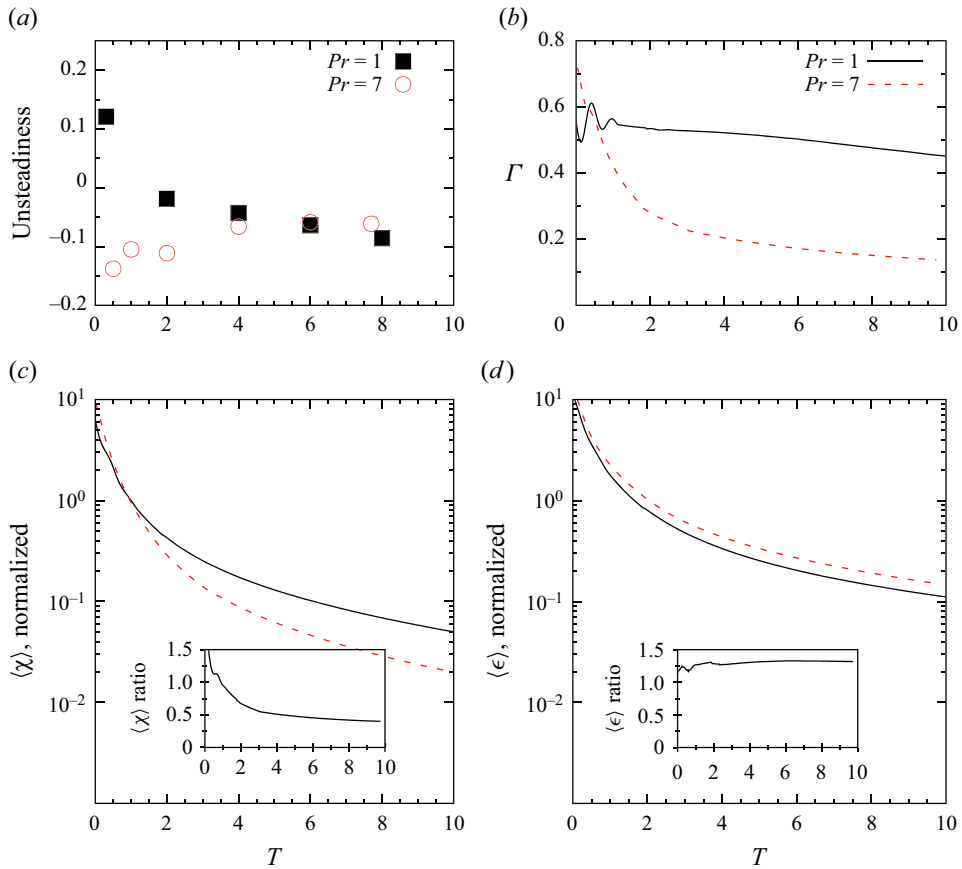


Figure 3. Results for (a) ‘unsteadiness’ which is $\partial_t \langle \|\mathbf{B}\|^2 \rangle / \langle \mathcal{P}_{B1} \rangle$ computed via the sum of the terms on the right-hand side of (2.14), (b) mixing coefficient $\Gamma \equiv \langle \chi \rangle / \langle \epsilon \rangle$, (c) $\langle \chi \rangle$ normalized by its value for $Pr = 1$ at $T = 1$ (in order to be able to compare the effect of Pr in the stratified case with that for the unstratified case shown in figure 1(a)), (d) $\langle \epsilon \rangle$ normalized by its value for $Pr = 1$ at $T = 1$. The inset plots in (c) and (d) show $\langle \chi \rangle_{Pr=7} / \langle \chi \rangle_{Pr=1}$ and $\langle \epsilon \rangle_{Pr=7} / \langle \epsilon \rangle_{Pr=1}$. In (b), the value for $Pr = 7$ and later times is consistent with that typically assumed for the ocean whereas the value for $Pr = 1$ is much higher.

5.2. Stably stratified turbulence

We now turn to consider the results for stably stratified turbulence. One immediate difference between the DNS for passive scalars and stably stratified turbulence is that in the former, the large scales are quasi-stationary, whereas in the latter they are decaying. However, under Kolmogorov’s quasi-equilibrium hypothesis we anticipate that the small scales of the flow that dominate the velocity and scalar gradients will be in a state of quasi-equilibrium. To test this, in figure 3(a) we plot the sum of the terms on the right-hand side of the equation for $\partial_t \langle \|\mathbf{B}\|^2 \rangle$ normalized by $\langle \mathcal{P}_{B1} \rangle$, as a function of ‘buoyancy time’ $T \equiv Nt / (2\pi)$. The results show that after an initial transient, the magnitude of $\partial_t \langle \|\mathbf{B}\|^2 \rangle / \langle \mathcal{P}_{B1} \rangle$ takes on values < 0.1 that are similar for both Pr cases. This indicates that the scalar gradients are indeed in a state of quasi-equilibrium. Therefore, the time dependence of the large-scale flow in the decaying stratified DNS should not cause significant differences for the scalar gradients compared with the passive scalar DNS, and any differences should be due to differences in the basic dynamics of the two cases.

In figure 3(b) we plot the mixing coefficient $\Gamma \equiv \langle \chi \rangle / \langle \epsilon \rangle$, and the results show that after the initial transient, Γ reduces dramatically as Pr is increased from 1 to 7. Figure 3(c) and (d) show $\langle \chi \rangle$ and $\langle \epsilon \rangle$, respectively, normalized by their values for $Pr = 1$ at $T = 1$. The results show that as Pr is increased from 1 to 7, $\langle \chi \rangle$ decreases while $\langle \epsilon \rangle$ increases. The insets in these plots show the ratios $\langle \chi \rangle_{Pr=7} / \langle \chi \rangle_{Pr=1}$ and $\langle \epsilon \rangle_{Pr=7} / \langle \epsilon \rangle_{Pr=1}$ in order to show more clearly the size of the variations. The results show that after the initial transient, $\langle \chi \rangle$ decreases by roughly 50% as Pr is increased from 1 to 7, while $\langle \epsilon \rangle$ increases by roughly 25%. This very strong reduction in $\langle \chi \rangle$ for stratified turbulence as Pr is increased is in stark contrast to what was observed earlier for the passive scalar runs where $\langle \chi \rangle$ varied by only $\approx 6\%$ as Pr was increased from 1 to 7.

At $T = 1.5$, when $\langle \chi \rangle$ has already dropped by $\approx 25\%$ in going from $Pr = 1$ to $Pr = 7$, the activity parameter $Gn \equiv \langle \epsilon \rangle / (\nu N^2)$ is ≈ 20 . This would usually be taken to suggest that buoyancy is playing a sub-leading role in the behaviour of the small-scale gradients that govern $\langle \chi \rangle$, and that the scalar gradients behave like those for a passive scalar. If this were the case, then the model of Donzis *et al.* (2005) would apply, according to which $\langle \chi \rangle$ will decrease with increasing Pr for $Pr \geq 1$ due to the emergence of the viscous–convective range, unless Re_λ is sufficiently high. Since the value of Re_λ in our DNS of stratified turbulence is much smaller (at $T = 0$, $Re_\lambda = 335$) than that in the DNS of passive scalars shown earlier (where $Re_\lambda = 633$), perhaps the much stronger Pr dependence of $\langle \chi \rangle$ for the stratified runs compared with the passive scalar runs is simply due to Re_λ being much smaller in the former and not due to the effect of buoyancy. To test this we used the model of Donzis *et al.* (2005) with the values of Re_λ in our DNS of stratified turbulence and found that their model predicts $\lesssim 14\%$ reduction of $\langle \chi \rangle$ (the reduction predicted depends on time since Re_λ is a function of time in the stratified flow) in going from $Pr = 1$ to $Pr = 7$. This variation is far smaller than the $\approx 50\%$ reduction we observe in figure 3(c). Hence, although the effect of the viscous–convection regime, which is captured in the model of Donzis *et al.* (2005), may play a role in explaining why $\langle \chi \rangle$ reduces in our stratified flow when going from $Pr = 1$ to $Pr = 7$, it is certainly not the main cause.

According to the analysis of § 3.2, a strong dependence of $\langle \chi \rangle$ on Pr will arise when the mean gradient production term $\langle \mathcal{P}_{B2} \rangle$ plays a sufficiently large role in the equation governing $\langle \|\mathbf{B}\|^2 \rangle$. To test this argument, we first consider in figure 4(a) the quantity $\langle \mathcal{P}_{B2} \rangle / \sigma_A^3$. In agreement with the analysis of § 2.2 (which also applies to the stratified case, as explained in § 3), the mean gradient production term $\langle \mathcal{P}_{B2} \rangle$ is positive at $t \ll \tau_\eta$ (this is only observable for the $Pr = 1$ case; we do not have data at small enough T for the $Pr = 7$ case to observe it), but then becomes negative once the ramp-cliff structures have emerged. The analysis in § 3.2 suggests that at least in the weakly stratified regime, the magnitude of $\langle \mathcal{P}_{B2} \rangle$ will grow with increasing Pr while $Pr \leq O(Pr_S)$, and we estimated $Pr_S = O(100)$. The results in figure 4(a) confirm this expected behaviour, which was also confirmed earlier for the passive scalar limit $\lambda_S \rightarrow 0$. The fact that the dependence of $\langle \chi \rangle$ on Pr is much stronger for the stratified case than for the passive scalar case must be due to $\langle \mathcal{P}_{B2} \rangle$ playing a much more significant role in the former case than the latter. To test this, in figure 4(b) we plot $\langle \mathcal{P}_{B2} \rangle / \langle \mathcal{P}_{B1} \rangle$. For the passive scalar case, this ratio was shown to be $O(10^{-3})$, and hence the impact of $\langle \mathcal{P}_{B2} \rangle$ on $\langle \chi \rangle$ is irrelevant for passive scalars. By contrast, the results in figure 4(b) show that for the stratified turbulent flows the magnitude of $\langle \mathcal{P}_{B2} \rangle / \langle \mathcal{P}_{B1} \rangle$ reaches values that are up to $O(1)$. This is fully consistent with the argument that it is the mechanism associated with $\langle \mathcal{P}_{B2} \rangle$ that is responsible for $\langle \chi \rangle$ exhibiting a much stronger dependence on Pr for stratified turbulence than for passive scalars.

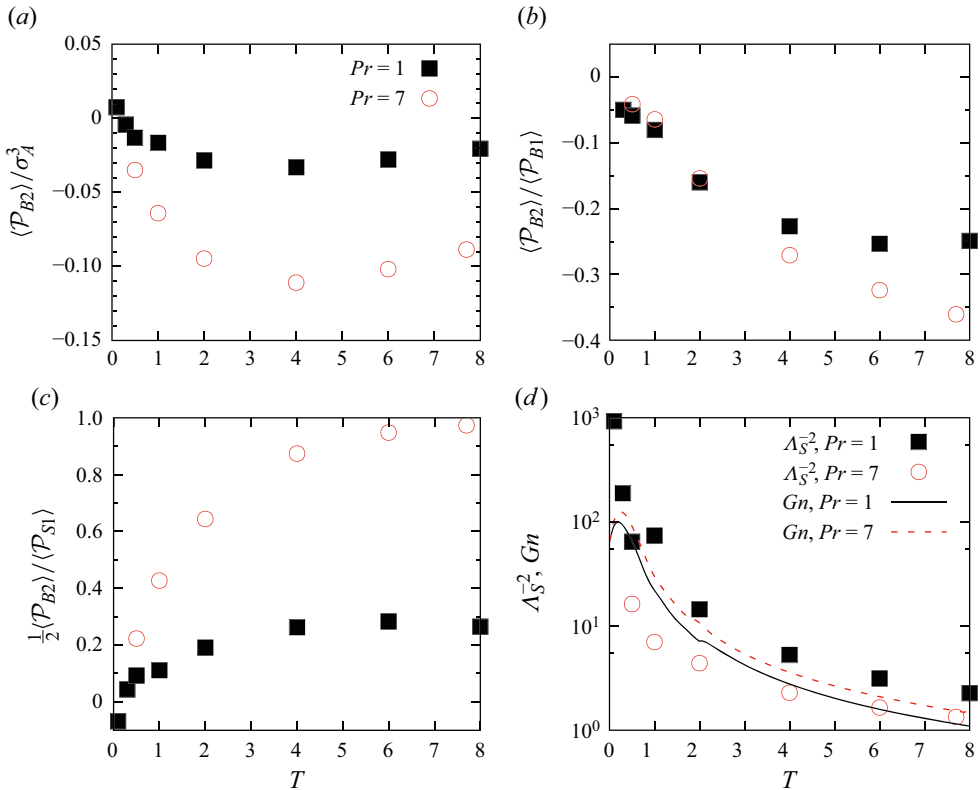


Figure 4. Results for (a) $\langle \mathcal{P}_{B2} \rangle / \sigma_A^3$, (b) $\langle \mathcal{P}_{B2} \rangle / \langle \mathcal{P}_{B1} \rangle$, (c) $(1/2) \langle \mathcal{P}_{B2} \rangle / \langle \mathcal{P}_{S1} \rangle$ and (d) Λ_S^{-2} and Gn . Each plot shows the data for $Pr = 1$ and $Pr = 7$.

The mechanism associated with $\langle \mathcal{P}_{B2} \rangle$ can only remain important for $\langle \chi \rangle$ when $\langle \mathcal{P}_{B2} \rangle / \langle \mathcal{P}_{B1} \rangle$ is not negligible. The scaling discussed in § 2 suggests that $\langle \mathcal{P}_{B2} \rangle / \langle \mathcal{P}_{B1} \rangle \sim O(\Lambda_B)$, and Λ_B decreases as Pr increases. This was confirmed for the passive scalars in figure 1, and the results in figure 4(b) confirm this in the stratified flows for $T \lesssim 2$. However, at longer times, the magnitude of $\langle \mathcal{P}_{B2} \rangle / \langle \mathcal{P}_{B1} \rangle$ increases with increasing Pr . The failure of the scaling prediction in this case could either be due to the buoyancy Reynolds number of the flow at these times being too small for the scaling to be appropriate, or else it could be due to the dependence of geometrical alignments on Pr that are not accounted for in the scaling estimate $\langle \mathcal{P}_{B2} \rangle / \langle \mathcal{P}_{B1} \rangle \sim O(\Lambda_B)$ (see detailed discussion in § 3.2). Associated with this is the fact that in Riley *et al.* (2023), it was shown that the ramp-cliff structures become stronger in stratified flows as Pr increases, the opposite of the behaviour for passive scalars (Sreenivasan 2018; Buaria *et al.* 2021a; Shete *et al.* 2022). Understanding the cause for this difference must be explored in future work, however, for the present discussion, the significant thing is that it could suggest that in stratified turbulent flows, $\langle \mathcal{P}_{B2} \rangle / \langle \mathcal{P}_{B1} \rangle$ may not become negligible ever for very large Pr .

To test that $\langle \mathcal{P}_{B2} \rangle$ is also the mechanism responsible for $\langle \epsilon \rangle$ increasing with increasing Pr , in figure 4(c) we plot $(1/2) \langle \mathcal{P}_{B2} \rangle / \langle \mathcal{P}_{S1} \rangle$. The ratio is positive and reaches values of $O(1)$, showing that $\langle \mathcal{P}_{B2} \rangle$ makes a significant contribution in aiding the nonlinear production term $\langle \mathcal{P}_{S1} \rangle$ in amplifying the strain rates in the flow. Moreover, $(1/2) \langle \mathcal{P}_{B2} \rangle / \langle \mathcal{P}_{S1} \rangle$ increases with Pr , consistent again with the argument that $\langle \mathcal{P}_{B2} \rangle$ is responsible for the increase of $\langle \epsilon \rangle$ with increasing Pr .

In § 3.3 it was argued that the relative size of the buoyancy to inertial forces in the equation for \mathbf{S} is given by Λ_S . The traditional way to estimate the importance of buoyancy at the smallest scales of the flow is through some kind of buoyancy Reynolds number, and we argued that for $Pr \sim O(1)$, $\Lambda_S \sim O(Gn^{-1/2})$, where Gn is the activity parameter, which is one way of defining a buoyancy Reynolds number. The standard argument is that $Gn \gg 1$ is the regime for which the impact of buoyancy at the small scales should be negligible. In figure 4(d) we plot Λ_S^{-2} and Gn evaluated for the stratified flows with $Pr = 1$ and $Pr = 7$. Consistent with the results in figure 4(c), the results show that Λ_S^{-2} decreases as Pr is increased, indicating that buoyancy plays an increasingly important role in the dynamics governing \mathbf{S} as Pr is increased. On the other hand, the results in figure 4(d) also show that Gn increases in going from $Pr = 1$ to $Pr = 7$, which would incorrectly suggest that the impact of buoyancy on the dynamics of the smallest flow scales reduces as Pr is increased. Therefore, Λ_S , rather than Gn , should be used as the metric for estimating the importance of buoyancy on the smallest scales in a stratified flow.

According to the argument presented in § 2.2, the reason why $\langle \mathcal{P}_{B2} \rangle$ transitions from being positive at $t \ll \tau_\eta$ to negative at later times is due to the emergence of ramp-cliff structures in the flow which are associated with a preference for $\mathbf{e}_B \equiv \mathbf{B}/\|\mathbf{B}\|$ to be aligned with \mathbf{e}_z . More specifically, the argument is that $\langle \mathcal{P}_{B2} \rangle$ becoming negative is associated with $\mathbf{e}_B \cdot \mathbf{e}_z > 0$ events being more probable than $\mathbf{e}_B \cdot \mathbf{e}_z < 0$ events (when $\gamma < 0$) due to the mechanism that generates the ramp-cliff structures. To test this, in figure 5 we plot the p.d.f. of $\mathbf{e}_B \cdot \mathbf{e}_z$, namely $\varphi(\mathbf{e}_B \cdot \mathbf{e}_z)$, for the stratified flows as well as the passive scalar results for reference. The stratified results for $Pr = 1$ show a clear bias towards $\mathbf{e}_B \cdot \mathbf{e}_z > 0$ events, consistent with the argument in § 2.2. As T increases the p.d.f. reduces and becomes more uniform over the central region of the space $\mathbf{e}_B \cdot \mathbf{e}_z \in [-1, +1]$, while it increases and becomes less uniform closer to the edges of the space. This suggests that as T increases and the flow becomes increasingly stratified, the conditions required for the generation of the ramp-cliff structures are only satisfied in extreme regions of the flow where the behaviour of \mathbf{B} differs strongly from its mean-field behaviour. The results for $Pr = 7$ show similar behaviour, except that the asymmetry of $\varphi(\mathbf{e}_B \cdot \mathbf{e}_z)$ is weaker than for $Pr = 1$. Interestingly, however, the results in Riley *et al.* (2023) for the same data set show that the skewness of B_z becomes stronger in going from $Pr = 1$ and $Pr = 7$. This difference reflects the fact that while the skewness of B_z is directly connected to asymmetry in $\varphi(\mathbf{e}_B \cdot \mathbf{e}_z)$, their dependence on Pr can differ because the skewness of B_z is influenced by the magnitudes of B_z whereas the alignments $\mathbf{e}_B \cdot \mathbf{e}_z$ are not.

For the passive scalars which are in the statistically stationary regime, the results in figure 5 also show that $\mathbf{e}_B \cdot \mathbf{e}_z > 0$ events are the most probable for $Pr = 1$. However, the bias towards $\mathbf{e}_B \cdot \mathbf{e}_z > 0$ events becomes weaker in going from $Pr = 1$ to $Pr = 7$, and this is consistent with previous results that show that for fixed Re , the ramp cliffs become weaker as Pr is increased beyond one (Sreenivasan 2018; Buaria *et al.* 2021a; Shete *et al.* 2022). It is interesting to note, however, that the results for $Pr = 7$ show that $\varphi(\mathbf{e}_B \cdot \mathbf{e}_z)$, while only weakly non-uniform for $|\mathbf{e}_B \cdot \mathbf{e}_z| \lesssim 0.9$, is strongly non-uniform for $|\mathbf{e}_B \cdot \mathbf{e}_z| > 0.9$. This residual preferential alignment is likely due to extreme regions of the flow with weak fluctuating scalar gradients where $\|\mathbf{B}\| \leq O(N)$ even though $\sigma_B \gg N$, since in such regions the mean-scalar gradient would still influence \mathbf{B} . However, the probability of such regions becomes vanishingly small for $\Lambda_B \equiv N/\sigma_B \rightarrow 0$, in which limit we would expect a uniform p.d.f. $\varphi(\mathbf{e}_B \cdot \mathbf{e}_z)$.

Further insights into the role of buoyancy on the velocity gradient dynamics can be obtained by considering the relative importance of the nonlinear amplification and buoyancy terms in regions classified by the invariant Q . Regions where $Q > 0$ are

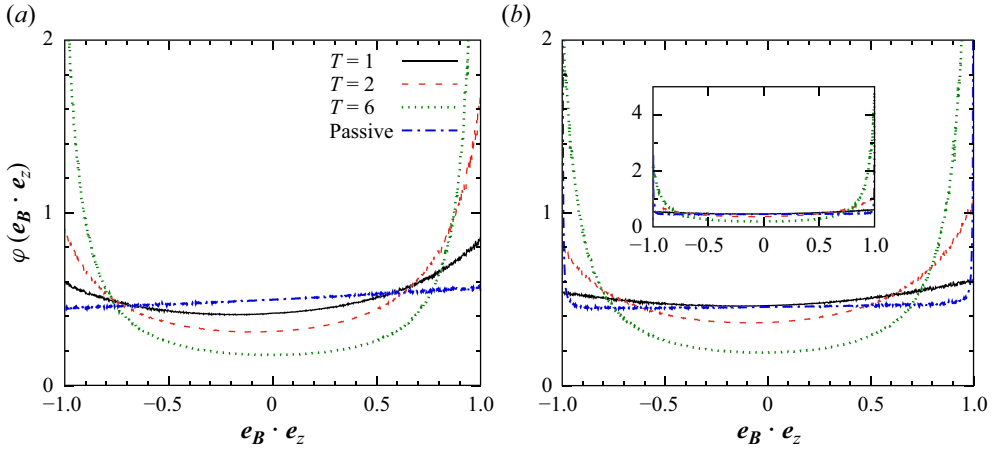


Figure 5. Results for the probability density function of $\mathbf{e}_B \cdot \mathbf{e}_z$ for (a) $Pr = 1$ and (b) $Pr = 7$. Stratified results are shown for different buoyancy times T .

rotation (or vorticity) dominated regions, while $Q < 0$ are strain dominated regions. The contributions to $\langle \mathcal{P}_{A1} \rangle$ (defined in (2.18)) and $\langle \mathcal{P}_{B2} \rangle$ from different regions may be considered using the decompositions

$$\langle \mathcal{P}_{A1} \rangle = \int_{\mathbb{R}} \varphi(Q) \langle \mathcal{P}_{A1} \rangle_Q dQ, \tag{5.3}$$

$$\langle \mathcal{P}_{B2} \rangle = \int_{\mathbb{R}} \varphi(Q) \langle \mathcal{P}_{B2} \rangle_Q dQ, \tag{5.4}$$

where $\varphi(Q)$ is the p.d.f. of Q . In a neutrally buoyant flow, $\langle \mathcal{P}_{A1} \rangle_Q$ would be positive for $Q > 0$ because of the prevalence of vortex stretching over vortex compression, and for $Q < 0$, $\langle \mathcal{P}_{A1} \rangle_Q$ should also be positive but now because of the prevalence of strain self-amplification over against suppression, which is associated with the intermediate eigenvalue of the strain-rate tensor being positive on average (Tsinober 2001; Tsinober, Vedula & Teung 2001). On the other hand, while the integral of $\varphi(Q) \langle \mathcal{P}_{B2} \rangle_Q$ over all Q is negative, there is no reason why $\varphi(Q) \langle \mathcal{P}_{B2} \rangle_Q$ must be negative for all Q . If it is not, then this would mean that buoyancy can have opposite effects on velocity gradient amplification in strain and rotation dominated regions of the flow.

In figure 6 we plot $\sigma_A^{-1} \varphi(Q) \langle \mathcal{P}_{A1} \rangle_Q$ and $-\sigma_A^{-1} \varphi(Q) \langle \mathcal{P}_{B2} \rangle_Q$, whose integrals over all Q yield $\langle \mathcal{P}_{A1} \rangle$ and $-\langle \mathcal{P}_{B2} \rangle$, respectively. Consistent with the behaviour in neutral flows, the results imply that in most cases, $\langle \mathcal{P}_{A1} \rangle_Q$ is positive for all Q , and so in both strain and vorticity dominated regions of stratified turbulence, the average effect of \mathcal{P}_{A1} is to amplify the velocity gradients. However, for $Pr = 1$ and $Q > 0$, the quantity $\sigma_A^{-1} \varphi(Q) \langle \mathcal{P}_{A1} \rangle_Q$ decreases significantly with increasing T , and at $T = 6$ it becomes negative for $Q/\sigma_Q \gtrsim 2$. This implies that in regions where the vorticity is largest, vortex compression is dominating over vortex stretching, and this is why $\sigma_A^{-1} \varphi(Q) \langle \mathcal{P}_{A1} \rangle_Q$ steadily reduces for $Q > 0$ as time advances. By contrast, for the $Pr = 7$ case, $\sigma_A^{-1} \varphi(Q) \langle \mathcal{P}_{A1} \rangle_Q$ is almost independent of time for $Q > 0$.

For $Pr = 1$, the values of $\sigma_A^{-1} \varphi(Q) \langle \mathcal{P}_{A1} \rangle_Q$ are significantly larger for $Q < 0$ than for $Q > 0$, and this is associated with velocity gradient production being stronger in strain dominated regions than in vorticity dominated regions (which is in turn the reason why

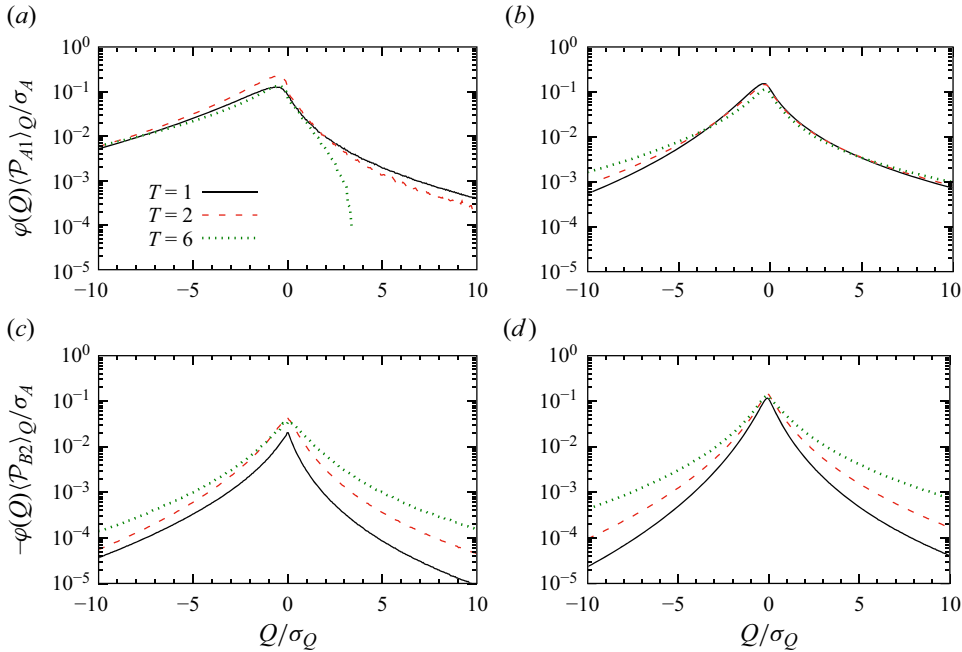


Figure 6. Results for (a,b) $\sigma_A^{-1} \varphi(Q) \langle \mathcal{P}_{A1} \rangle_Q$ and (c,d) $-\sigma_A^{-1} \varphi(Q) \langle \mathcal{P}_{B2} \rangle_Q$ from stratified DNS. Panels (a,c) are for $Pr = 1$, panels (b,d) are for $Pr = 7$ and different curves are for different buoyancy times T . Note that for $Pr = 1$, $\sigma_A^{-1} \varphi(Q) \langle \mathcal{P}_{A1} \rangle_Q$ becomes negative at $T = 6$ for $Q/\sigma_Q \gtrsim 2$.

strain self-amplification makes a larger contribution than vortex stretching to the kinetic energy cascade (Carbone & Bragg 2020; Johnson 2020, 2021), which is also the case in stratified turbulence Zhang *et al.* 2022). For $Pr = 7$, where the effects of buoyancy on the velocity gradient dynamics are stronger than for $Pr = 1$, we see that $\sigma_A^{-1} \varphi(Q) \langle \mathcal{P}_{A1} \rangle_Q$ is much more symmetric with respect to Q . Compared with the $Pr = 1$ case, velocity gradient production in strain dominated regions is much weaker, and that in vorticity dominated regions is much stronger for $Pr = 7$.

The results for $-\sigma_A^{-1} \varphi(Q) \langle \mathcal{P}_{B2} \rangle_Q$ reveal that $\langle \mathcal{P}_{B2} \rangle_Q$ is in fact positive for all Q , meaning that buoyancy acts as a source for velocity gradients in both strain and vorticity dominated regions of the flow. Comparing $-\sigma_A^{-1} \varphi(Q) \langle \mathcal{P}_{B2} \rangle_Q$ for $Pr = 1$ and $Pr = 7$ shows that the function increases significantly at almost all Q as Pr is increased, just as was shown to occur for the mean value $-\langle \mathcal{P}_{B2} \rangle$. Therefore, increasing Pr causes the buoyancy production term to grow not only in regions of relatively low Q/σ_Q (which dominate $-\langle \mathcal{P}_{B2} \rangle$), but also in regions of large fluctuations where $|Q/\sigma_Q| \gg 1$. In figure 4(c) it was shown that for $Pr = 7$, $(1/2) \langle \mathcal{P}_{B2} \rangle$ and $\langle \mathcal{P}_{S1} \rangle$ (the latter being equal to $(1/2) \langle \mathcal{P}_{A1} \rangle$) are of the same order for $T \gtrsim 1$. However, the results for $\sigma_A^{-1} \varphi(Q) \langle \mathcal{P}_{A1} \rangle_Q$ and $-\sigma_A^{-1} \varphi(Q) \langle \mathcal{P}_{B2} \rangle_Q$ show that the former is generally much larger than the latter when $|Q/\sigma_Q| \gg 1$ and $T \geq 1$. This means that during large fluctuations of the velocity gradients, the nonlinear amplification mechanism \mathcal{P}_{A1} dominates over the buoyancy contribution $-\mathcal{P}_{B2}$. This is easily understood from the fact that the definition of \mathcal{P}_{A1} involves \mathbf{A} to the power of three, while \mathcal{P}_{B2} involves \mathbf{A} to the power of one, and therefore \mathcal{P}_{A1} grows much more rapidly than \mathcal{P}_{B2} when $Q \equiv -\mathbf{A} \cdot \mathbf{A}/2$ is driven to large values.

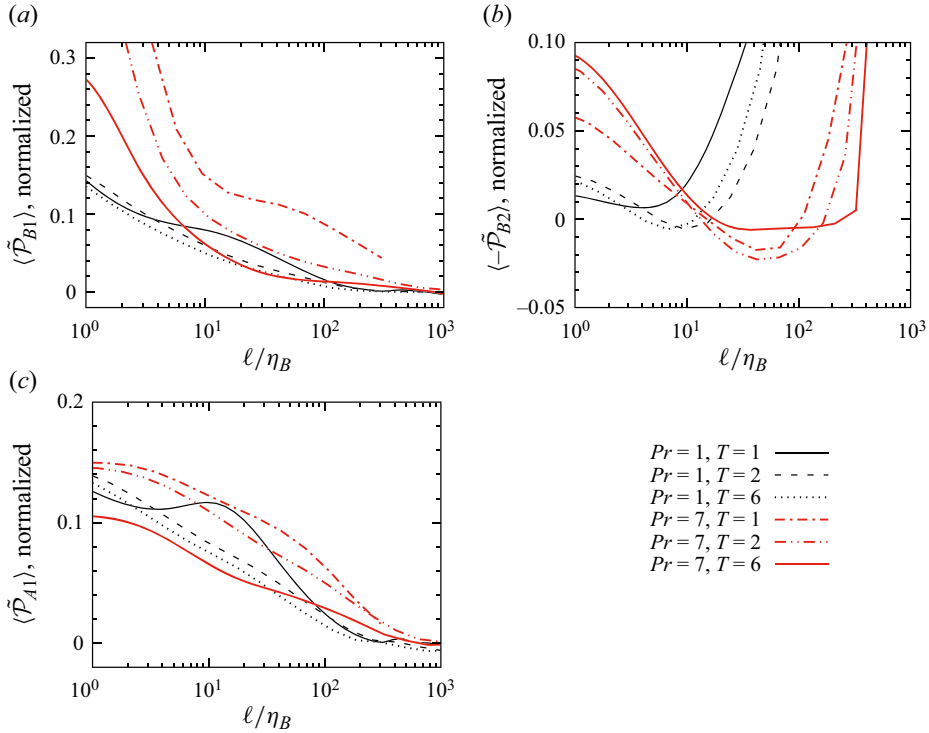


Figure 7. Results for the filtered production terms (a) $\langle \tilde{\mathcal{P}}_{B1} \rangle \equiv -\langle \tilde{\mathbf{B}} \cdot \tilde{\mathbf{A}}^\top \cdot \tilde{\mathbf{B}} \rangle$, (b) $\langle \tilde{\mathcal{P}}_{B2} \rangle \equiv \Lambda_B \langle \tilde{\mathbf{B}} \cdot \tilde{\mathbf{A}}^\top \cdot \mathbf{e}_z \rangle$, (c) $\langle \tilde{\mathcal{P}}_{A1} \rangle \equiv -\langle \tilde{\mathbf{A}}^\top : (\tilde{\mathbf{A}} \cdot \tilde{\mathbf{A}}) \rangle$. Quantities are normalized using $\sigma_{\tilde{\mathbf{A}}}^3$, where $\sigma_{\tilde{\mathbf{A}}} \equiv \sqrt{\langle \|\tilde{\mathbf{A}}\|^2 \rangle}$.

Finally, in § 3 we argued that the filtered buoyancy production term $-\langle \tilde{\mathcal{P}}_{B2} \rangle \equiv -N \langle \tilde{\mathbf{B}} \cdot \tilde{\mathbf{A}}^\top \cdot \mathbf{e}_z \rangle$ will change sign as the filter length ℓ increases in a stationary flow. In particular, for $\lim_{\ell/\eta_B \rightarrow 0} \langle \tilde{\mathcal{P}}_{B2} \rangle \rightarrow \langle \mathcal{P}_{B2} \rangle$, which is negative, but when ℓ/η_B becomes large enough for $|\langle \tilde{\mathcal{P}}_{B1} \rangle| \ll |\langle \tilde{\mathcal{P}}_{B2} \rangle|$ then $\langle \tilde{\mathcal{P}}_{B2} \rangle$ must become positive because in this range it must act as the dominant source term in the equation for $\langle \|\tilde{\mathbf{B}}\|^2 \rangle$ in the stationary regime. The implication of this is that in the equation for $\langle \|\tilde{\mathbf{A}}\|^2 \rangle$, the buoyancy term $-\langle \tilde{\mathcal{P}}_{B2} \rangle$ acts as a source term at sufficiently small ℓ/η_B , while it acts as a sink term at large ℓ/η_B . To test this, in figure 7 we plot $\langle \tilde{\mathcal{P}}_{B1} \rangle \equiv -\langle \tilde{\mathbf{B}} \cdot \tilde{\mathbf{A}}^\top \cdot \tilde{\mathbf{B}} \rangle$, $\langle \tilde{\mathcal{P}}_{B2} \rangle \equiv N \langle \tilde{\mathbf{B}} \cdot \tilde{\mathbf{A}}^\top \cdot \mathbf{e}_z \rangle$ and $\langle \tilde{\mathcal{P}}_{A1} \rangle \equiv -\langle \tilde{\mathbf{A}}^\top : (\tilde{\mathbf{A}} \cdot \tilde{\mathbf{A}}) \rangle$, normalized using $\sigma_{\tilde{\mathbf{A}}}^3$, where $\sigma_{\tilde{\mathbf{A}}} \equiv \sqrt{\langle \|\tilde{\mathbf{A}}\|^2 \rangle}$.

The results show that $\langle \tilde{\mathcal{P}}_{B1} \rangle$ and $\langle \tilde{\mathcal{P}}_{A1} \rangle$ are positive at all scales in the flow, and so act as source terms at all scales in the equations for $\langle \|\tilde{\mathbf{B}}\|^2 \rangle$ and $\langle \|\tilde{\mathbf{A}}\|^2 \rangle$, respectively. The results for $\langle \tilde{\mathcal{P}}_{B2} \rangle$ for the stratified DNS show that this term changes sign as ℓ/η_B is increased, such that the buoyancy term $-\langle \tilde{\mathcal{P}}_{B2} \rangle$ acts as a source term for $\langle \|\tilde{\mathbf{A}}\|^2 \rangle$ at small scales, but as a sink term at larger scales. Although this agrees with the prediction from § 3, the conditions under which the sign change is observed to occur disagrees with those predicted by the analysis. In particular, although $\langle \tilde{\mathcal{P}}_{B2} \rangle$ becomes positive as ℓ/η_B increases, it becomes negative again at even larger ℓ/η_B , even though $|\langle \tilde{\mathcal{P}}_{B1} \rangle| \ll |\langle \tilde{\mathcal{P}}_{B2} \rangle|$ at these larger scales. This disagreement is, however, almost certainly due to the fact that the analysis in § 3 applies to a stationary flow, whereas the DNS for stratified flow is decaying. As a result, in view of the analysis in § 2.3, $\langle \tilde{\mathcal{P}}_{B2} \rangle$ need not be positive at scales where $|\langle \tilde{\mathcal{P}}_{B1} \rangle| \ll |\langle \tilde{\mathcal{P}}_{B2} \rangle|$

in order to balance $\langle \tilde{\mathbf{B}} \cdot \nabla \nabla \cdot \boldsymbol{\tau}_\phi \rangle$ because of the contribution from $\partial_t \langle \|\tilde{\mathbf{B}}\|^2 \rangle < 0$ which is significant at larger scales in the decaying flow.

For the passive scalar cases (not shown), $\langle \tilde{\mathcal{P}}_{B2} \rangle$ remains negative at all scales, which is contrary to expectation based on the analysis in § 2.3. The most likely reason for this discrepancy is that since $\lim_{\ell/\eta_B \rightarrow 0} N/\sqrt{\langle \|\tilde{\mathbf{B}}\|^2 \rangle} = N/\sqrt{\langle \|\mathbf{B}\|^2 \rangle}$ is very small for the passive scalar cases, then the condition under which $\langle \tilde{\mathcal{P}}_{B2} \rangle$ is predicted to become positive, namely $N/\sqrt{\langle \|\tilde{\mathbf{B}}\|^2 \rangle} \geq O(1)$, may only occur at $\ell = O(L)$. At such filter scales, the data for $\langle \tilde{\mathcal{P}}_{B2} \rangle \equiv N \langle \tilde{\mathbf{B}} \cdot \tilde{\mathbf{A}}^\top \cdot \mathbf{e}_z \rangle$ will be strongly affected by statistical noise due to the box size because, although theoretically $\lim_{\ell/L \rightarrow \infty} \tilde{\mathbf{B}} \rightarrow \mathbf{0}$ and $\lim_{\ell/L \rightarrow \infty} \tilde{\mathbf{A}} \rightarrow \mathbf{0}$ for a homogeneous flow, in practice these limiting behaviours may be approximately satisfied for $\ell \geq O(L)$. A much larger domain may therefore be required to observe $\langle \tilde{\mathcal{P}}_{B2} \rangle$ becoming positive for the passive scalar case in order to minimize the effects of statistical noise at $\ell = O(L)$, as well as to more fully satisfy the assumptions made in the theoretical analysis of a statistically stationary, homogeneous flow.

6. Conclusions

This study was primarily motivated by recent DNSs of stably stratified turbulence that showed that as Pr is increased from 1 to 7, the mean TPE dissipation rate $\langle \chi \rangle$ drops dramatically, while the mean TKE dissipation rate $\langle \epsilon \rangle$ increases significantly (Riley *et al.* 2023). To understand the mechanism responsible for this surprising behaviour, we analysed the equations governing the fluctuating strain rate \mathbf{S} and fluctuating density gradient \mathbf{B} . This was done for both passive scalars driven by a mean scalar gradient and stably stratified flows in order to understand the extent to which the behaviour observed for stratified flows is simply due to the effects of an imposed mean-scalar gradient vs the particular dynamical effects due to buoyancy forces. The predictions from the analysis were then compared with DNS results for passive scalars and stably stratified turbulence.

Production mechanisms in the equation for $\langle \|\mathbf{B}\|^2 \rangle$ (which is proportional to the mean-scalar dissipation rate $\langle \chi \rangle$) are associated with the stirring processes that intensify flow gradients, and the magnitude of the resulting gradients determines the mixing rates. Prandtl number effects on the mixing rates can therefore be understood at a fundamental level by examining the effects of Pr on the production mechanisms, of which there are two; one associated with \mathbf{B} , which we refer to as $\langle \mathcal{P}_{B1} \rangle$, and the other associated with the mean scalar gradient, which we refer to as $\langle \mathcal{P}_{B2} \rangle$. In the passive scalar context, we discussed that $\langle \mathcal{P}_{B1} \rangle$ is affected by a de-localization effect due to a disparity between the smallest scales of the velocity and scalar fields when $Pr \neq 1$. This de-localization effect renders $\langle \mathcal{P}_{B1} \rangle$ less effective in amplifying $\langle \|\mathbf{B}\|^2 \rangle$ as Pr is increased. We also argued that $\langle \mathcal{P}_{B2} \rangle$ actually opposes the amplification of $\langle \|\mathbf{B}\|^2 \rangle$, and that this is associated with the existence of ramp-cliff structures in the scalar field. The impact of this production term depends upon the parameter regime of the flow, but when it is important, its oppositional effect causes $\langle \chi \rangle$ to decrease with increasing Pr . Our DNS results for $Re_\lambda = 633$ and $Pr \in [0.1, 7]$ show that on average $\langle \mathcal{P}_{B2} \rangle$ does indeed oppose the production of $\langle \|\mathbf{B}\|^2 \rangle$, however, its contribution is negligible compared with $\langle \mathcal{P}_{B1} \rangle$. A weak dependence of $\langle \chi \rangle$ on Pr was observed which is mainly due to the de-localization effect associated with $\langle \mathcal{P}_{B1} \rangle$.

For stably stratified flows where the scalar field is the fluid density, the buoyancy term in the equation for $\langle \|\mathbf{S}\|^2 \rangle$ is equal to $-(1/2)\langle \mathcal{P}_{B2} \rangle$. Since $\langle \mathcal{P}_{B2} \rangle < 0$, then the effect of buoyancy is to amplify $\langle \|\mathbf{S}\|^2 \rangle$. This is surprising because in stably stratified flows, buoyancy is expected to suppress turbulent motion. However, by analysing the filtered

velocity gradient equation we demonstrated that while buoyancy amplifies the small-scale velocity gradients, it suppresses the large-scale velocity gradients. This analysis was confirmed using DNS, and is also connected with the observation in Legaspi & Waite (2020) based on numerical simulations that there is a transfer of potential to kinetic energy at the smallest scales in stably stratified turbulence.

Concerning the effect of Pr on $\langle \epsilon \rangle$ and $\langle \chi \rangle$ in stratified turbulence, we presented an analysis for the weakly stratified regime where the effects of buoyancy on $\langle \|\mathbf{S}\|^2 \rangle$ and $\langle \|\mathbf{B}\|^2 \rangle$ are perturbative. This analysis predicts that as Pr is increased, the term $\langle \mathcal{P}_{B2} \rangle$ should grow in magnitude, with the result that $\langle \epsilon \rangle$ should increase and $\langle \chi \rangle$ should decrease with increasing Pr , in qualitative agreement with the results in Riley *et al.* (2023). We also presented arguments that showed that this growth of $\langle \mathcal{P}_{B2} \rangle$ must saturate at some value $Pr = O(Pr_S)$ due to the smallest scales of the density field becoming isotropic in the limit $Pr \rightarrow \infty$, and we estimated that at minimum $Pr_S = O(100)$. Guided by the results and insights from the analysis, we used DNS data of stably stratified turbulence with $Pr = 1$ and $Pr = 7$ (the same data set used in Riley *et al.* 2023) to compute the production terms in the equations for $\langle \|\mathbf{S}\|^2 \rangle$ and $\langle \|\mathbf{B}\|^2 \rangle$ to see how they are impacted by Pr and how they differ from the passive scalar case. For $\langle \|\mathbf{B}\|^2 \rangle$, the results show that $\langle \mathcal{P}_{B2} \rangle$ is negative (i.e. opposes the growth of $\langle \|\mathbf{B}\|^2 \rangle$) and grows in magnitude as Pr increases, in agreement with the theoretical arguments. Moreover, it plays a much larger role in the equation for $\langle \|\mathbf{B}\|^2 \rangle$ in stratified flows than for passive scalars, supporting the argument that this term is the reason why $\langle \chi \rangle$ decreases strongly with increasing Pr in stratified turbulent flows. For $\langle \|\mathbf{S}\|^2 \rangle$, the DNS showed that the buoyancy term $-(1/2)\langle \mathcal{P}_{B2} \rangle$ is of the same sign and of the same order as the nonlinear amplification term, and the fact that $-(1/2)\langle \mathcal{P}_{B2} \rangle$ increases with increasing Pr is the reason why $\langle \epsilon \rangle$ increases with increasing Pr .

We also argued that the strong effect of Pr in stratified flows means that the activity parameter Gn (or any other standard definition of the buoyancy Reynolds number) may not provide a reliable way to estimate the impact of buoyancy on the smallest scales of stably stratified turbulence. By analysing the equation for \mathbf{S} , we proposed a new non-dimensional number Λ_S that compares the buoyancy and inertial terms in this equation and captures the effect of Pr . Using DNS data we showed that while Λ_S correctly predicts that when Pr increases, the effects of buoyancy at the smallest scales increase, Gn incorrectly predicts the opposite.

Finally, an analysis of the filtered gradient equations predicted that the mean density gradient term must change sign at sufficiently large scales, such that buoyancy will act as a source for velocity gradients at small scales, but as a sink at large scales. Our DNS confirmed that there is indeed a range of scales where this buoyancy term becomes negative, however, the conditions under which this is observed to occur do not agree with those predicted by the theoretical analysis. We argued that this is most likely because, while the analysis assumes a statistically stationary flow, the DNS is for decaying stratified turbulence. At larger scales where the time derivative term is significant in the filtered gradient equations, this changes the dominant balance of the equations relative to the stationary case, and therefore the scale at which the buoyancy term will change sign.

The analysis suggests that in the limit $\Lambda_S \rightarrow 0$, the velocity and density gradient fields in stratified turbulent flows will behave like those for a neutral flow where density is passive. In this regime, $\langle \epsilon \rangle$ will become independent of Pr , as will $\langle \chi \rangle$ if the large-scale Reynolds number of the flow Re is also sufficiently high. However, DNS at higher Re and Pr are needed in order to understand how quickly this asymptotic regime is attained, and therefore whether $\langle \epsilon \rangle$ and $\langle \chi \rangle$ might become independent of Pr in parameter regimes relevant to real stratified flows. Another important topic to be explored in future work is how the

results and insights from this work that focuses on the gradient field dynamics connects to the multiscale behaviour of the kinetic and potential energy fields in stratified flows. In particular, does the positive contribution of buoyancy to the production of fluctuating velocity gradients imply that at the smallest scales potential energy is transferred back to the kinetic energy field, and if so, over what scales does this occur and how does it depend on Pr ?

Acknowledgements. This research used resources of the Oak Ridge Leadership Computing Facility at the Oak Ridge National Laboratory, which is supported by the Office of Science of the U.S. Department of Energy under Contract No. DE-AC05-00OR22725. Additional resources were provided through the U.S. Department of Defense High Performance Computing Modernization Program by the Army Engineer Research and Development Center and the Army Research Laboratory under Frontier Project FP-CFD-FY14-007.

Funding. A.D.B. was supported by National Science Foundation (NSF) CAREER award # 2042346. S.deB.K. was supported by U.S. Office of Naval Research grant number N00014-19-1-2152.

Declaration of interests. The authors report no conflict of interest.

Author ORCIDs.

 Andrew D. Bragg <https://orcid.org/0000-0001-7068-8048>;

 Stephen M. de Bruyn Kops <https://orcid.org/0000-0002-7727-8786>.

REFERENCES

- ASHURST, W.T., KERSTEIN, A.R., KERR, R.M. & GIBSON, C.H. 1987 Alignment of vorticity and scalar gradient with strain rate in simulated Navier–Stokes turbulence. *Phys. Fluids* **30**, 2343.
- BATCHELOR, G.K. 1959 Small-scale variation of convected quantities like temperature in turbulent fluid. Part 1. General discussion and the case of small conductivity. *J. Fluid Mech.* **5**, 113.
- BETCHOV, R. 1956 An inequality concerning the production of vorticity in isotropic turbulence. *J. Fluid Mech.* **1** (05), 497–504.
- BRAGG, A.D. & DE BRUYN KOPS, S.M. 2024 Asymptotic analysis of mixing in stratified turbulent flows, and the conditions for an inertial sub-range. [arXiv:2402.10704](https://arxiv.org/abs/2402.10704).
- DE BRUYN KOPS, S.M. & RILEY, J.J. 1998 Direct numerical simulation of laboratory experiments in isotropic turbulence. *Phys. Fluids* **10** (9), 2125–2127.
- DE BRUYN KOPS, S.M. & RILEY, J.J. 2019 The effects of stable stratification on the decay of initially isotropic homogeneous turbulence. *J. Fluid Mech.* **860**, 787–821.
- BUARIA, D., CLAY, M.P., SREENIVASAN, K.R. & YEUNG, P.K. 2021a Small-scale isotropy and ramp-cliff structures in scalar turbulence. *Phys. Rev. Lett.* **126**, 034504.
- BUARIA, D., CLAY, M.P., SREENIVASAN, K.R. & YEUNG, P.K. 2021b Turbulence is an ineffective mixer when Schmidt numbers are large. *Phys. Rev. Lett.* **126**, 074501.
- CARBONE, M. & BRAGG, A.D. 2020 Is vortex stretching the main cause of the turbulent energy cascade? *J. Fluid Mech.* **883**, R2.
- CARBONE, M., IOVIENO, M. & BRAGG, A.D. 2020 Symmetry transformation and dimensionality reduction of the anisotropic pressure hessian. *J. Fluid Mech.* **900**, A38.
- CHERTKOV, M., PUMIR, A. & SHRAIMAN, B.I. 1999 Lagrangian tetrad dynamics and the phenomenology of turbulence. *Phys. Fluids* **11** (8), 2394–2410.
- CHEVILLARD, L. & MENEVEAU, C. 2006 Lagrangian dynamics and statistical geometric structure of turbulence. *Phys. Rev. Lett.* **97** (17), 174501.
- CORRSIN, S. 1951 On the spectrum of isotropic temperature fluctuations in an isotropic turbulence. *J. Appl. Phys.* **22**, 469–472.
- DANISH, M. & MENEVEAU, C. 2018 Multiscale analysis of the invariants of the velocity gradient tensor in isotropic turbulence. *Phys. Rev. Fluids* **3**, 044604.
- DIAMESSIS, P.J. & NOMURA, K.K. 2000 Interaction of vorticity, rate-of-strain, and scalar gradient in stratified homogeneous sheared turbulence. *Phys. Fluids* **12** (5), 1166–1188.
- DONZIS, D.A., SREENIVASAN, K.R. & YEUNG, P.K. 2005 Scalar dissipation rate and dissipative anomaly in isotropic turbulence. *J. Fluid Mech.* **532**, 199–216.

- FERACO, F., MARINO, R., PUMIR, A., PRIMAVERA, L., MININNI, P.D., POUQUET, A. & ROSENBERG, D. 2018 Vertical drafts and mixing in stratified turbulence: sharp transition with Froude number. *Europhys. Lett.* **123** (4), 44002.
- GARGETT, A., OSBORN, T. & NASMYTH, P. 1984 Local isotropy and the decay of turbulence in a stratified fluid. *J. Fluid Mech.* **144**, 231–280.
- GIBSON, C.H. 1980 Fossil turbulence, salinity, and vorticity turbulence in the ocean. In *Marine Turbulence* (ed. J.C.J. Nihous), pp. 221–257. Elsevier.
- GULITSKI, G., KholmYANSKY, M., KINZELBACH, W., LÜTHI, B., TSINOBER, A. & YORISH, S. 2007 Velocity and temperature derivatives in high-Reynolds-number turbulent flows in the atmospheric surface layer. Part 3. Temperature and joint statistics of temperature and velocity derivatives. *J. Fluid Mech.* **589**, 103–123.
- HOLZER, M. & SIGGIA, E.D. 1994 Turbulent mixing of a passive scalar. *Phys. Fluids* **6**, 1820–1837.
- JACKSON, P.R. & REHMANN, C.R. 2014 Experiments on differential scalar mixing in turbulence in a sheared, stratified flow. *J. Phys. Oceanogr.* **44** (10), 2661–2680.
- JOHNSON, P.L. 2020 Energy transfer from large to small scales in turbulence by multiscale nonlinear strain and vorticity interactions. *Phys. Rev. Lett.* **124**, 104501.
- JOHNSON, P.L. 2021 On the role of vorticity stretching and strain self-amplification in the turbulence energy cascade. *J. Fluid Mech.* **922**, A3.
- LEGASPI, J.D. & WAITE, M.L. 2020 Prandtl number dependence of stratified turbulence. *J. Fluid Mech.* **903**, 36 pages.
- LINDBORG, E. 2006 The energy cascade in a strongly stratified fluid. *J. Fluid Mech.* **550**, 207–242.
- MAFFIOLI, A., BRETTHOUWER, G. & LINDBORG, E. 2016 Mixing efficiency in stratified turbulence. *J. Fluid Mech.* **794**, R3.
- MARINO, R., FERACO, F., PRIMAVERA, L., PUMIR, A., POUQUET, A., ROSENBERG, D. & MININNI, P.D. 2022 Turbulence generation by large-scale extreme vertical drafts and the modulation of local energy dissipation in stably stratified geophysical flows. *Phys. Rev. Fluids* **7**, 033801.
- MENEVEAU, C. 2011 Lagrangian dynamics and models of the velocity gradient tensor in turbulent flows. *Annu. Rev. Fluid Mech.* **43** (1), 219–245.
- NAZARENKO, S. & LAVAL, J.-P. 2000 Non-local two-dimensional turbulence and batchelor’s regime for passive scalars. *J. Fluid Mech.* **408**, 301–321.
- NOMURA, K.K. & POST, G.K. 1998 The structure and dynamics of vorticity and rate of strain in incompressible homogeneous turbulence. *J. Fluid Mech.* **377**, 65–97.
- OBUKHOV, A.M. 1949 Structure of temperature field in a turbulent flow. *Izv. Akad. Nauk SSSR Geogr. Geofiz.* **13**, 58–69.
- OVERHOLT, M.R. & POPE, S.B. 1998 A deterministic forcing scheme for direct numerical simulations of turbulence. *Comput. Fluids* **27**, 11–28.
- POPE, S.B. 2000 *Turbulent Flows*. Cambridge University Press.
- RAO, K.J. & DE BRUYN KOPS, S.M. 2011 A mathematical framework for forcing turbulence applied to horizontally homogeneous stratified flow. *Phys. Fluids* **23**, 065110.
- RILEY, J.J. & DE BRUYN KOPS, S.M. 2003 Dynamics of turbulence strongly influenced by buoyancy. *Phys. Fluids* **15** (7), 2047–2059.
- RILEY, J.J., COUCHMAN, M.M.P. & DE BRUYN KOPS, S.M. 2023 The effect of Prandtl number on decaying stratified turbulence. *J. Turbul.* **0**, 1–19.
- RILEY, J.J. & LINDBORG, E. 2012 Recent progress in stratified turbulence. In *Ten Chapters in Turbulence* (ed. P.A. Davidson, Y. Kaneda & K.R. Sreenivasan), pp. 269–317. Cambridge University Press.
- RORAI, C., MININNI, P.D. & POUQUET, A. 2014 Turbulence comes in bursts in stably stratified flows. *Phys. Rev. E* **89**, 043002.
- SALEHIPOUR, H. & PELTIER, W.R. 2015 Diapycnal diffusivity, turbulent Prandtl number and mixing efficiency in Boussinesq stratified turbulence. *J. Fluid Mech.* **775**, 464–500.
- SHETE, K.P., BOUCHER, D.J., RILEY, J.J. & DE BRUYN KOPS, S.M. 2022 Effect of viscous-convective subrange on passive scalar statistics at high Reynolds number. *Phys. Rev. Fluids* **7** (2), 024601.
- SHETE, K.P. & DE BRUYN KOPS, S.M. 2020 Area of scalar isosurfaces in homogeneous isotropic turbulence as a function of Reynolds and Schmidt numbers. *J. Fluid Mech.* **883**, A38.
- SMYTH, W.D., MOUM, J.N. & CALDWELL, D.R. 2001 The efficiency of mixing in turbulent patches: inferences from direct simulations and microstructure observations. *J. Phys. Oceanogr.* **31**, 1969–1992.
- SREENIVASAN, K.R. 2018 Turbulent mixing: a perspective. *Proc. Natl Acad. Sci. USA* **2018**, 201800463.
- SUJOVOLSKY, N.E., MINDLIN, G.B. & MININNI, P.D. 2019 Invariant manifolds in stratified turbulence. *Phys. Rev. Fluids* **4**, 052402.

Understanding Prandtl number effects on turbulent mixing

- SUJOVOLSKY, N.E. & MININNI, P.D. 2020 From waves to convection and back again: the phase space of stably stratified turbulence. *Phys. Rev. Fluids* **5**, 064802.
- TOM, J., CARBONE, M. & BRAGG, A.D. 2021 Exploring the turbulent velocity gradients at different scales from the perspective of the strain-rate eigenframe. *J. Fluid Mech.* **910**, A24.
- TSINOBER, A. 2000 Vortex stretching versus production of strain/dissipation. In *Turbulence Structure and Vortex Dynamics*, pp. 164–191. Cambridge University Press.
- TSINOBER, A. 2001 *An Informal Introduction to Turbulence*. Kluwer Academic.
- TSINOBER, A., VEDULA, P. & TEUNG, P.K. 2001 Random Taylor hypothesis and the behavior of local convective accelerations in isotropic turbulence. *Phys. Fluids* **13**, 1974–1984.
- VIEILLEFOSSE, P. 1982 Local interaction between vorticity and shear in a perfect incompressible fluid. *J. Phys.* **43** (6), 837–842.
- ZHANG, X., DHARIWAL, R., PORTWOOD, G., DE BRUYN KOPS, S.M. & BRAGG, A.D. 2022 Analysis of scale-dependent kinetic and potential energy in sheared, stably stratified turbulence. *J. Fluid Mech.* **946**, A6.